UM-HE-71-22

THE UNIVERSITY OF MICHIGAN

COLLEGE OF LITERATURE, SCIENCE, AND THE ARTS
Department of Physics

Technical Report

DEUTERON SPIN ALIGNMENT IN DEUTERON-PROTON SCATTERING AT 3.6 GEV/C

Gerry Bunce

ORA Project 03454

supported by:

NATIONAL SCIENCE FOUNDATION
GRANT NO. GP-19257
WASHINGTON, D.C.

administered through:

OFFICE OF RESEARCH ADMINISTRATION ANN ARBOR

July 1971

ACKNOWLEDGEMENTS

First, I wish to thank Oliver Overseth who has guided my development in physics since I've been at Michigan. He has continually kept my needs in mind, and he initiated this experiment to give me a thesis project, allowing me considerable responsibility in its development.

Our co-workers on the experiment were Steve Olsen from Rockerfeller University, Lee Pondrom, Howard Halpern, and Bob Handler from the University of Wisconsin, and Jay Walker from the University of Michigan. (Jay also did the drawings in this thesis.) Also contributing to this experiment were John Barney and John Bauhm from Wisconsin.

The people at the Princeton-Pennsylvania Accelerator were very helpful and we made many friends there. I wish to thank Cortland Parker, Bob Barry, Al Dowe and the rest of the people there.

Developing a physics experiment, running and analyzing it, is a long and trying process. My wife Nan had a lot to do with stabilizing me and keeping things in perspective, as well as putting up with the moving, anxiety, etc.

People at Michigan who cheerfully gave me counsel were Gordy Kane, Jim Smith, Fred Harris, and Smith Powell. Lincoln Wolfenstein made many helpful suggestions during the analysis of the results.

TABLE OF CONTENTS

LIST OF FIGURES

LIST OF TABLES

ABSTRACT

DEUTERON SPIN ALIGNMENT IN
DEUTERON-PROTON SCATTERING AT 3.6 GEV/C

by

Gerry Michael Bunce

Chairman: O. E. Overseth

Proton-deuteron forward scattering just beyond the diffraction peak is expected to result mostly from the D-wave of the deuteron. Recoil deuterons from scattering in this region should be strongly spin aligned. D. R. Harrington suggested a double scattering experiment to observe this alignment. Using a 3.6 GeV/c external deuteron beam from the Princeton-Pennsylvania Accelerator, we spin aligned and analyzed deuterons in two scatters off of hydrogen. Deuteron polarization, both alignment and vector polarization, from the first scatter was measured by observing the up-right and right-left asymmetry of the deuterons in the second scatter. We observed scattering over four-momentum transfers from $-t = .13$ to $.54$ GeV$^2/c^2$. The up-right asymmetry reached 67% for small momentum transfers, and went to -37% for the largest scattering angle. The right-left asymmetry was generally 25% for all angles.

A calculation using the multiple scattering theory of Glauber with no free parameters gives the qualitative features of the up-right asymmetry observed, with a

maximum of 90% and the same shape as our data. Close agreement is not expected, since the calculation ignores spin-orbit effects and the target proton spin and thus makes no right-left asymmetry prediction. The up-right asymmetry prediction is quite sensitive to the parameterization for the free nucleon-nucleon scattering amplitudes. Treating the nucleon amplitude slopes and real parts as free parameters, we fit the theory to both the asymmetry data and the forward proton-deuteron cross section data at 1 GeV. Larger real parts (-70%) of the nucleon amplitudes are preferred than those reported from nucleon-nucleon scattering. The larger real parts bring the p-n cross sections found from p-d scattering into agreement with σ_{np} from neutron beam experiments and agree with multiple scattering model fits to other proton-nucleus scattering data at 1 GeV (p-He, p-C, p-O). Both the experimental results and the calculation are presented.

I. SYNOPSIS

The multiple scattering theory of R. J. Glauber[1] correctly predicts forward differential cross sections for high energy proton scattering off of nuclei such as carbon, helium, and oxygen. The theory describes nuclear scattering by a series of multiple scattering terms, each calculable given the free incident particle-nucleon scattering amplitudes and the nuclear wave function. The multiple scattering series consists of a single scattering term where only one internal nucleon is seen by the incident particle (the impulse approximation, or spectator model), a double scattering term where two internal nucleons are involved, etc. The single scattering term dominates at small scattering angles, exhibiting a sharp diffraction peak, while multiple scattering terms dominate at larger angles. Generally, the single and the succeeding multiple scattering terms interfere destructively, giving dips in cross section where the successive contributions are roughly equal. The dips are borne out nicely by experiment for p-He[2,3], p-C[2] and p-O[2] scattering.

Several years ago, calculations made for scattering off deuterium didn't fare as well (Figure 1). The predicted dip (the dashed lines in Figure 1) was not found experimentally for either πd[4,5] or pd[6,7] scattering. A number of explanations dealing with approximations used in the theory were put forward, but each lead to inconsistencies with successful predictions for other

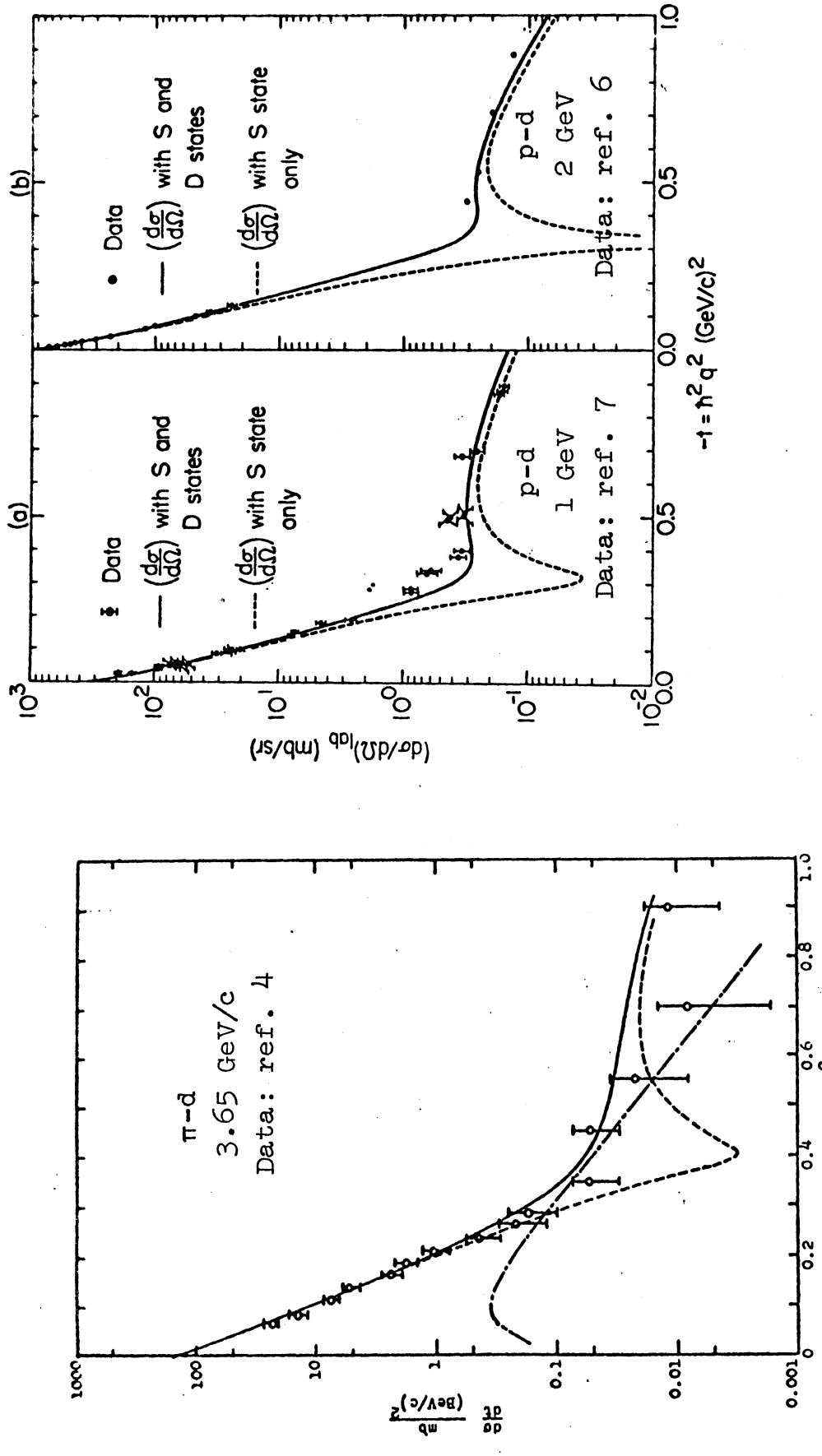

Figure 1. Analysis of pd^{10} and πd^{11} scattering. The dashed lines are fits without the D-wave, the solid lines include the D-wave.

experiments. In 1968 E. Coleman and T. G. Rhoades[8], and independently D. R. Harrington[9] showed that including the spin effects of the deuteron, the 7% D-wave, filled in the dip region (the solid lines of Figure 1). This explanation satisfied the πd and pd observations and didn't upset the successful predictions of Glauber theory, since the carbon, helium, and oxygen nuclei have zero spin.

If D-wave scattering is responsible for the shoulder in the cross section, scattering in this region should be strongly spin dependent. The tensor term in the deuteron wave function prefers scattering where the spins lie in a plane perpendicular to the momentum transfer in the single scattering region. This could be observed with a polarized deuteron target[10], but it is difficult to achieve the necessary degree of polarization. To test the pd spin dependence, Harrington reversed the reference frame and suggested a double scattering experiment using a deuteron beam scattered twice off hydrogen[12]. The first scatter would align the spins in a plane perpendicular to the momentum transfer, and the second scatter would analyze this alignment. Such an alignment would be described by a $\cos 2\varphi$ term (φ is the azimuth of the second scatter) representing an up-right form of asymmetry. The experiment would test the multiple scattering theoretical description of the pd spin effects and could yield

information on the deuteron wave function and the two nucleon-nucleon scattering amplitudes.

We performed this experiment at the Princeton-Pennsylvania Accelerator. The accelerator furnished a high intensity external deuteron beam of 10^{12}/second at a momentum of 3.6 Gev/c, equivalent to a past pd scattering experiment[7] at 1 Gev kinetic energy. The deuteron beam was scattered off a ten inch hydrogen target, producing a 10^{4}/second secondary elastic deuteron beam (Figure 2). Elastic scattering was well defined by a simple magnet-slit system--everything else scattered at 8° has a considerably lower momentum than the elastic deuterons. The first target was pushed up and down the beam line to define different momentum transfers.

For the second hydrogen target, the momentum transfer was defined by the recoil proton range in polyethylene. A particle with the proper range coincident with a forward particle in the correct quadrant (proton up with deuteron down, say) triggered four wire spark chambers (Figure 2). The counters and chambers covered the full 360° of azimuth. The analyzer was set throughout the experiment at a four momentum transfer-squared value of

$$-t_b = .23 \pm .015 \text{ Gev}^2/c^2 .$$

The data consisted of trajectories of the forward triggering particles, seen in the wire chambers. With about half background, the $\cos 2\varphi$ or up-right asymmetry

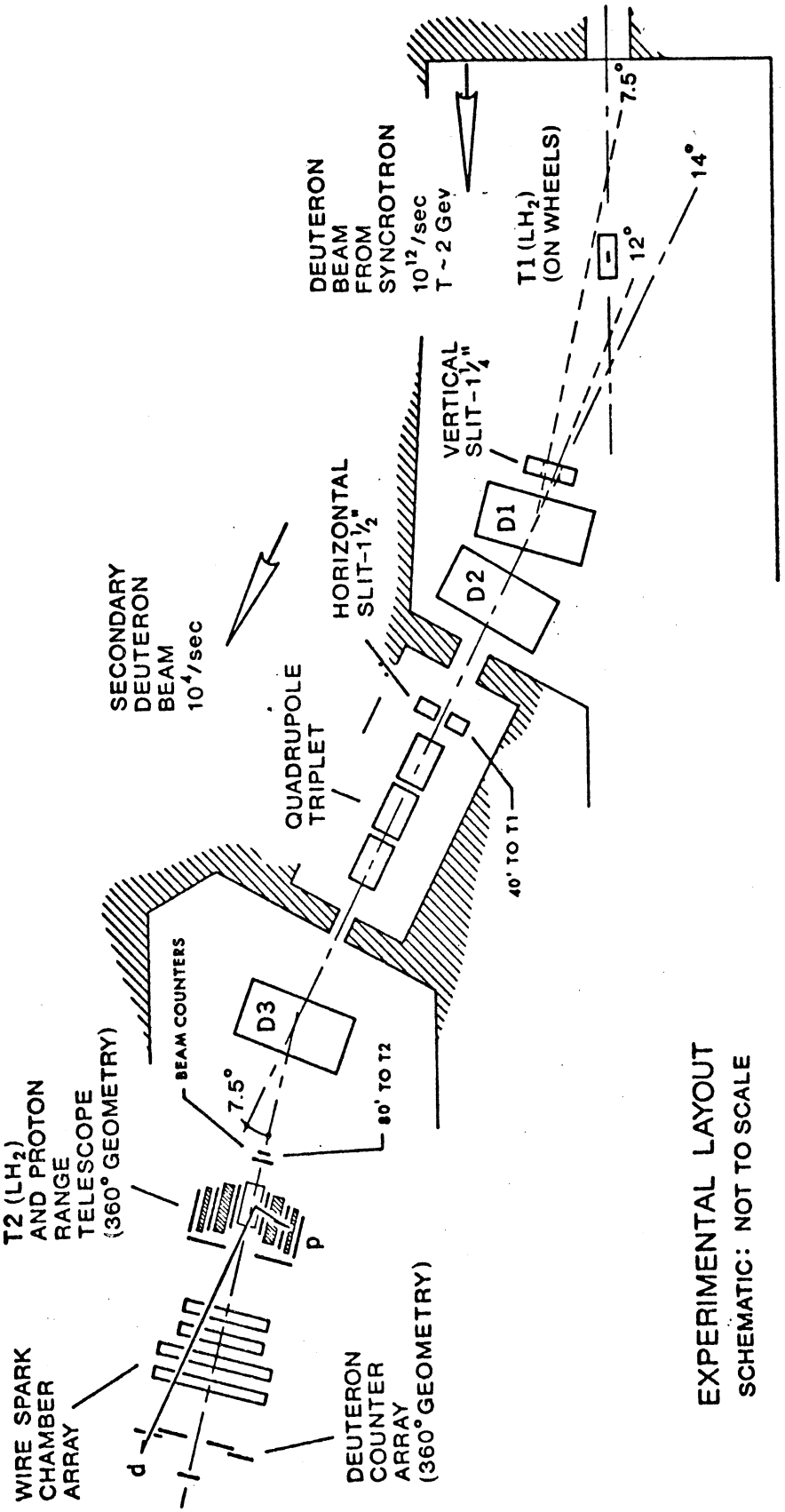

Figure 2. Schematic of experimental area.

was quite large. The $\cos 2\varphi$ asymmetry after background subtractions has the same shape as the asymmetry in the raw data, plotted against the first scatter momentum transfer. The $\cos 2\varphi$ asymmetry has a maximum of .67, crosses zero at $-t_a = .41$ Gev$^2/c^2$ and becomes negative.

The multiple scattering calculation, ignoring the spin-orbit effects, has the same qualitative shape as the data, but with a $\cos 2\varphi$ asymmetry rising to .88 and crossing zero at $-t_a = .38$. The calculation uses no free parameters. Now, the spin-orbit effects should be important. At these energies, pp and np polarizations are large--on the order of 30 to 40%. Including the nucleon spin leads to possible vector polarization in the scattering, giving a left-right or $\cos\varphi$ asymmetry upon analysis, as well as affecting the $\cos 2\varphi$ asymmetry. Indeed, we found a $\cos\varphi$ term of .25, generally constant in the first scatter momentum transfer. Thus, the spin-orbit effects are clearly important.

So, scattering in this momentum transfer region is strongly spin dependent, as predicted by the multiple scattering theory. The theory gives the qualitative shape of the data, even neglecting the spin-orbit effects. The shape of the predicted up-right asymmetry is more dependent on the parameterization of the nucleon-nucleon scattering amplitudes than on the deuteron wave function. These free nucleon-nucleon scattering amplitudes must be the same as those used in multiple scattering

fits to proton-nucleus forward cross sections at 1 Gev (pd, pHe, pC, pO). The amplitudes are parameterized as gaussians, normalized to the optical point:

$$f_{NN}(q) = \frac{k_{cm}\sigma_{NN}}{4\pi}(i + \alpha_{NN})\, e^{-b_{NN}|t|/2}$$

where NN represents either the pp or the np scattering amplitude, σ_{NN} are the total cross sections, b_{NN} are the slopes, and α_{NN} are the ratios of real to imaginary parts for the respective amplitudes. In fitting the multiple scattering theory to the asymmetry data and to the forward proton-nucleus cross sections, we find somewhat smaller slopes and larger negative α_{NN}'s are preferred than those reported from pp and np scattering. More definite results must await a calculation using the added nucleon spin dependence.

A discussion of the multiple scattering calculation, the experimental aspects, and the detailed results follow in separate sections.

II. THE ALIGNMENT PREDICTIONS

A spin-1 double scattering experiment can generally yield both $\cos 2\varphi$ and $\cos\varphi$ asymmetries in the azimuth. The $\cos\varphi$ asymmetry results mostly from vector polarization where the spin up population along a particular axis differs from the spin down population, as in spin-$\frac{1}{2}$ double scattering. The $\cos 2\varphi$ asymmetry arises from spin alignment in the scattering--the $\text{spin}_z=0$ substate does not contain one third of the total number of beam particles (a non-oriented beam can be described as having one third of its number in each of the magnetic substates). The spin alignment of a beam along an axis is

$$\text{Alignment} = \frac{(N_+ + N_-) - 2N_0}{N_+ + N_- + N_0}$$

where the beam has N_+, N_0, N_- particles with spin projections 1, 0, -1 on the axis. When the $\text{spin}_z=0$ state is depleted, we find the maximum alignment of +1. If both scatters have alignments near +1, the $\cos 2\varphi$ asymmetry can be near 100%.

The Glauber multiple scattering theory can be used to obtain predictions for alignment versus scattering angle and, thus, for the double scattering asymmetry. Historically, the multiple scattering theory encountered problems with both pd and πd scattering, leading to the introduction of the deuteron spin into the theory. The spin-orbit effects and the spin of the incident particle were left out to simplify matters, as we do here. With this

approximation, the multiple scattering theory predicts nearly complete alignment and a $\cos 2\varphi$ asymmetry close to +1 for optimum scattering angles. No vector polarization can occur, given that the spin-orbit effects are ignored, and the $\cos\varphi$ asymmetry would be zero. Also, no alignment would be possible from the spherical wave function of the deuteron, due to the assumption above.

A. Multiple Scattering Theory

The Glauber multiple scattering theory provides a framework for describing high energy particle scattering off nuclei. The deuteron-proton interaction is described in the deuteron rest frame as a sum of a single-scatter contribution (where the proton hits off either of the two nucleons of the deuteron, with the deuteron sticking together) and a double scatter contribution (the proton hits off both nucleons). The first term is the impulse approximation of Chew[13], and the second term is a very successful second order correction due to Glauber[1]. If all spins are ignored, the two terms are essentially out of phase with one another. When the overall amplitude is squared to obtain the cross section, a negative single-double scattering interference term results. This interference term nearly zeroes the differential cross section (for a spherical deuteron) at the angle where single and double scattering exchange dominence. It is here that the non-spherical part of the deuteron wave

function, the D-wave, dominates and fills in the dip in cross section. The spin dependence of scattering in this angular range is quite strong.

The term

$$f_1(q) = f_{pn}(q)S(\vec{q}/2) + f_{pp}(q)S(-\vec{q}/2)$$

represents single scattering. $\vec{q}$ is the momentum transferred to the proton, f_{NN} is the amplitude for nucleon-nucleon scattering at angle q, S(q/2) is the form factor for the deuteron giving the probability that the spectator nucleon happens to be moving in direction $\vec{q}$ (q/2 arises because the fermi momentum distribution is in the rest frame of the deuteron). One nucleon knocked in the direction $\vec{q}$ and the spectator nucleon moving in direction $\vec{q}$ results in an elastic interaction--the deuteron sticks together.

The double scattering term is

$$f_2(q) = \frac{i}{2\pi k}\int f_{NN}(\vec{q}/2 + \vec{q}')f_{NN}(\vec{q}/2 - \vec{q}')S(\vec{q}')d^2q' \ .$$

For this, a sum is taken over the possible combinations of double scatters which yield an elastic interaction. A small angle approximation accounts for the summation over the impact parameter plane (d^2q'), rather than three space.

The deuteron form factor may be written[10,14]

$$S(\vec{q},\vec{J}) = S_0(q) - S_2(q)[3(\vec{J}\cdot\hat{q})^2 - 2]/\sqrt{2} \ .$$

S_0 is the spherical form factor and S_2 the quadrupole

form factor and $\vec{J}$ is the deuteron spin operator. With the deuteron spin included in the theory, one talks of the scattering amplitudes above as operators, summing over initial and final spin states to obtain the scattering matrix. If we write the deuteron wave function as

$$\psi_M(r) = 1/\sqrt{4\pi}\ (\ u(r)/r + w(r)/r/8\ S_{12}\ )\ \chi_M$$

the deuteron form factors are

$$S_0(q) = \int (u^2 + w^2)\ j_0(qr)\ dr$$
$$S_2(q) = \int 2(uw - w^2/\sqrt{8}\ )\ j_2(qr)\ dr \quad .$$

Now, the quadrupole form factor S_2 dominates the dip region. This term (see page 10) prefers spins perpendicular to the momentum transfer $\vec{q}$ to spins along $\vec{q}$. The deuteron spins tend to lie in a plane perpendicular to the momentum transfer. A second scatter at the same angle would produce more scattering perpendicular to this plane than parallel to it, i. e. more scattering along the original momentum transfer axis. This is the origin of the $\cos 2\varphi$ asymmetry. This happens because the tensor term in the deuteron wave function, S_{12}, prefers spins along $\vec{r}$, the axis joining the two nucleons. The form factor, weighted by $e^{i\vec{q}\cdot\vec{r}}$, prefers $\vec{q} \perp \vec{r}$ and thus $\vec{q} \perp \vec{J}$.

Spin dependent scattering is described by a density matrix formed from the nine matrix elements of the scattering amplitude operator:

$$M_{ij} = \langle i|\ f_{op}(\vec{q})\ |j\rangle \quad .$$

i,j are the final and initial deuteron spin projections on the spin axis z. A particular set of quantization axes $\vec{x},\vec{y},\vec{z}$ must be chosen relative to the real space

axes defined in the scatter $\vec{k},\vec{q},\vec{n}=\vec{k}x\vec{q}$. In general we have for the single scattering term

$$M_{ij}(\vec{q})_1 = \langle i|\ f_{1op}(\vec{q})\ |j\rangle$$
$$= (f_{pn}(q) + f_{pp}(q))(S_0(q/2)\delta_{ij} + S_2(q/2)\langle i|\ [3(\vec{J}\cdot\hat{q})^2 - 2]\ |j\rangle//2$$

and for the double scattering term

$$M_{ij}(\vec{q})_2 = \langle i|\ f_{2op}\ |j\rangle$$
$$= \frac{i}{2\pi k}\int f_{np}f_{pp}S_0(q')d^2q'\delta_{ij} + \langle i|\frac{i}{2\pi k}\int f_{np}f_{pp}S_2(q')[3(\vec{J}\cdot\vec{q}')^2-2]d^2q'|j\rangle//2$$
$$= \frac{i}{2\pi k}\int f_{np}f_{pp}S_0(q')d^2q'\delta_{ij} + \frac{i}{2\pi k}\int f_{np}f_{pp}S_2(q')d^2q'\langle i|3(\vec{J}\cdot\vec{k})^2-2|j\rangle//2 \quad .$$

For the quadrupole double scattering term, assuming gaussians with the same slope for each of the nucleon-nucleon scattering amplitudes, the only angular dependence in the two dimensional integral appears in the operator. It has been integrated through in the second step.

If we arbitrarily choose the set of spin quantization axes $\vec{x}=\vec{q}$, $\vec{y}=\vec{n}$, $\vec{z}=\vec{k}$, the matrix elements are quite simple:

$$M_{11} = M + \tfrac{1}{2}Q$$
$$M_{00} = M - Q$$
$$M_{1-1} = M_{-11} = -3/2\ Q1$$
$$M_{i0} = M_{0i} = 0 \qquad i=\pm 1 \ .$$

M is the spherical scattering amplitude consisting of a single and a double scattering term

$$M = M1 + M2$$

$$M1 = f_{np}(q)S_0(q/2) + f_{pp}(q)S_0(-q/2)$$

$$M2 = \frac{i}{2\pi k}\int d^2q' f_{np}f_{pp}S_0(q') \quad ,$$

while Q is the quadrupole scattering amplitude:

$$Q = Q1 + Q2$$

$$Q1 = f_{np}(q)S_2(q/2)/\sqrt{2} + f_{pp}(q)S_2(-q/2)/\sqrt{2}$$

$$Q2 = \frac{i}{2\pi k}\int d^2q' f_{np}f_{pp}S_2(q')/\sqrt{2} \quad .$$

The f_{NN} may be written as simple gaussians,

$$f_{NN}(q) = \frac{k\sigma_{NN}}{4\pi}(i + \alpha_{NN})\, e^{-b_{NN}q^2/2}$$

and experiment fixes the six parameters σ_{NN}, α_{NN}, b_{NN}. The multiple scattering calculation is made in the deuteron rest frame. k is the target proton wave number in this frame, while q is the lab momentum transfer (taking $-t=q^2$ is a good approximation for small q[15]). The nucleon parameters for 1 Gev pN scattering and the deuteron form factors are in Table 1. The double scattering integrals reduce to

$$\begin{matrix} M2 \\ Q2 \end{matrix} = \frac{i}{2\pi k} f_{np}(q/2)f_{pp}(q/2) \begin{matrix} I_0 \\ I_2 \end{matrix}$$

with

$$\begin{matrix} I_0 \\ I_2 \end{matrix} = \int d^2q'\, e^{-(b_{np}+b_{pp})q'^2/2} \begin{matrix} S_0(q') \\ S_2(q')/\sqrt{2} \end{matrix} \quad .$$

The integrals are given in the table. The f_{NN} are mostly imaginary, S_0 and S_2 are real. Thus, the spherical and quadrupole amplitudes M and Q are mostly imaginary. The imaginary parts of M, Q, Q1 and the deuteron form factors are plotted in Figure 3. When the quadrupole terms are ignored, a dip in cross section would appear at $-t=.37$.

$$\sigma_{pn} = 40 \text{ mb} \qquad \sigma_{pp} = 47.5 \text{ mb}$$

$$b_{pn} = 4.1 \text{ (Gev/c)}^{-2} \qquad b_{pp} = 6.4 \text{ (Gev/c)}^{-2}$$

$$k = 2.729 \text{ mb}^{-1/2}$$

$$S_0(q) = \sum_i A_i \, e^{-\alpha_i q^2}$$

$$S_2(q)//2 = q^2 \sum_i B_i \, e^{-\beta_i q^2}$$

with

	A_i	α_i	B_i	β_i
i = 1	-.038	1.871	2.518	79.13
i = 2	.338	12.33	2.034	20.58
i = 3	.695	64.59	.3956	5.575

(α_i, β_i, B_i in (Gev/c)^{-2})

$$I_0 = 2.5\,\pi \sum_i A_i \frac{1}{b_{ave} + \alpha_i} \text{ mb}^{-1} = .187 \text{ mb}^{-1}$$

$$I_2 = 2.5\,\pi \sum_i B_i \frac{1}{(b_{ave} + \beta_i)^2} \text{ mb}^{-1} = .053 \text{ mb}^{-1}$$

where

$$b_{ave} = (b_{pn} + b_{pp})/2$$

Table 1. The nucleon-nucleon scattering parameters are from the Particle Data Group compilation[16]. The deuteron form factors are given by G. Alberi, et al.[17] I_0 and I_2 are defined in the text.

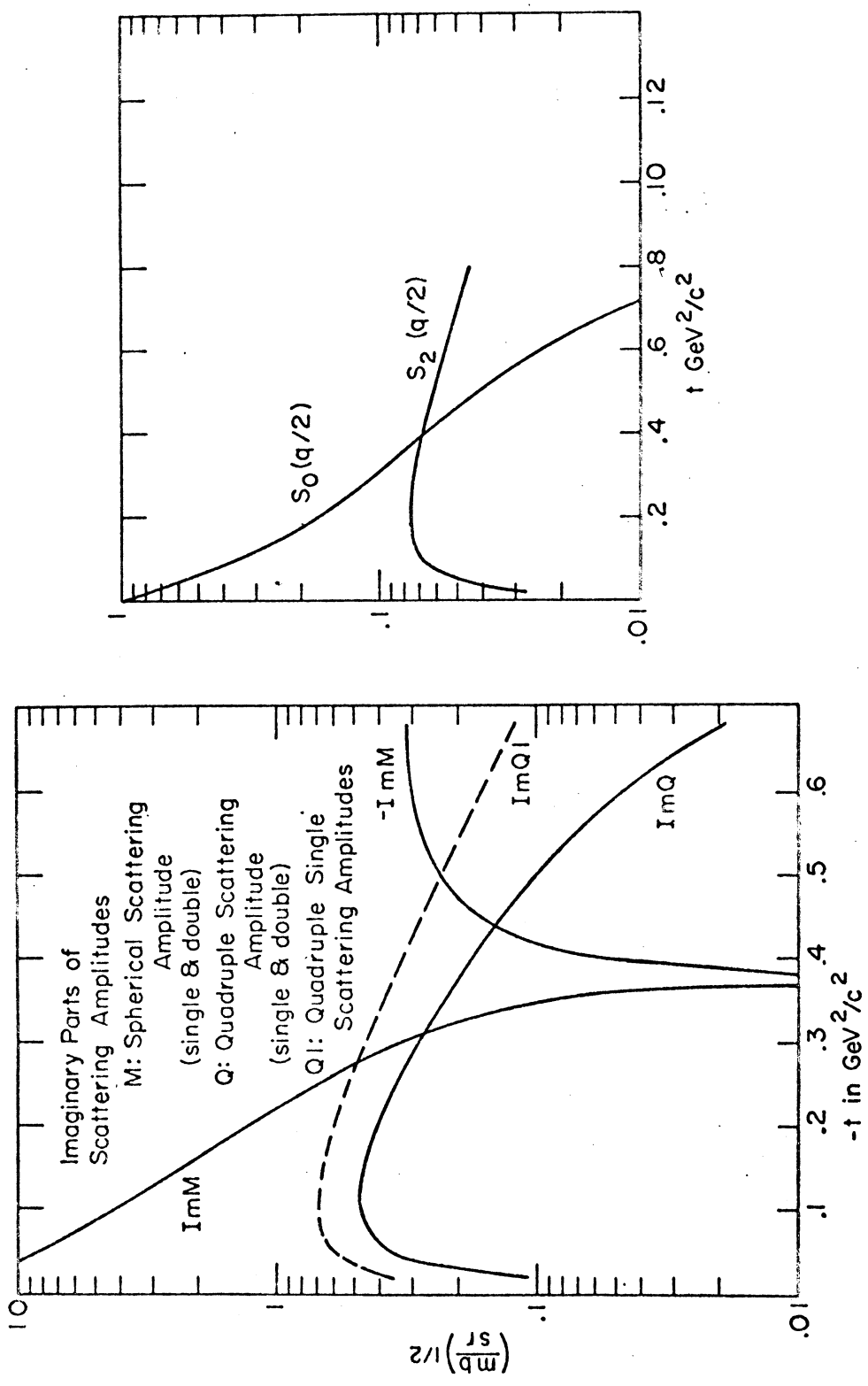

Figure 3. The imaginary parts of the deuteron scattering amplitudes and the deuteron form factors S_0 and S_2, as defined in the text.

We must introduce the density matrix to describe the spin dependence of the scattering.

B. The Density Matrix

A secondary beam of particles produced in a spin dependent scatter is usually a mixed beam which cannot be represented with a single wave function. The density matrix is a mathematical device which describes the spin states present in the beam.

The generalization to spin dependence is straight forward[18]. The wave function for a spin-dependent scatter may be written in the form

$$\psi(r) = \chi_1 e^{i\vec{k}\cdot\vec{r}} + M\chi_1 \frac{e^{ikr}}{r} \quad .$$

M is a scattering matrix replacing $f(\theta)$ and χ_1 is a three row spinor describing the initial spin state. This wave function represents a pure beam. For a mixed beam, we must average over the pure spin vectors χ_1, which is accomplished by the density matrix:

$$\rho_1 = \sum_{r=1}^{3} \omega_r \chi_{1r} \chi_{2r}^{\dagger} \quad .$$

ω_r is the weight of the spin state χ_{1r} in the beam.

An equally weighted sum over the three possible eigenstates describes a non-aligned deuteron beam:

$$\rho_1 = 1/3 \begin{pmatrix} 1 \\ 0 \\ 0 \end{pmatrix}^{(100)} + 1/3 \begin{pmatrix} 0 \\ 1 \\ 0 \end{pmatrix}^{(010)} + 1/3 \begin{pmatrix} 0 \\ 0 \\ 1 \end{pmatrix}^{(001)}$$

or

$$\rho_1 = 1/3\ I = 1/3 \ , \ \mathrm{tr}\ \rho_1 = 1 \quad .$$

If there are N_+ particles in the beam with spin projection up along the z axis, etc.,

$$\rho = \begin{pmatrix} N_+ & & \\ & N_0 & \\ & & N_- \end{pmatrix}$$

and $$\text{tr } \rho = N_+ + N_0 + N_-$$

is the intensity of the beam. (The other matrix elements depend on the spin projections along the x and y axes of the spin quantization system.) The cross section is just the intensity of the secondary beam divided by the incident beam intensity

$$d\sigma/d\Omega = \text{tr } \rho_2/\text{tr } \rho_1 .$$

The density matrix for the secondary beam follows from the form of the scattered wave,

$$\begin{aligned} \rho_2 &= \chi_2\chi_2^\dagger \\ &= (M\chi_1)(M\chi_1)^\dagger \\ &= M\chi_1\chi_1^\dagger M^\dagger \\ &= M\rho_1 M^\dagger , \end{aligned}$$

the last step being an extension of the definition for the mixed beam. Therefore, the cross section for the scattering of an unpolarized beam is

$$d\sigma/d\Omega = 1/3 \text{ tr } M^\dagger M ,$$

the spin dependent replacement for $|f(\theta)|^2$.

It is more meaningful to expand the 3x3 density matrix in terms of operators whose expectation values represent the intensity, vector polarization, and spin alignment of the beam[19]. The nine operators are

$$\hat{1},\ \hat{P}_x,\ \hat{P}_y,\ \hat{P}_z,\ \hat{P}_{xy},\ \hat{P}_{xz},\ \hat{P}_{yz},\ \hat{P}_{xx}-\hat{P}_{yy},\ \hat{P}_{xx}+\hat{P}_{yy}(=\hat{P}_{zz})$$

where $\hat{P}_i = \hat{S}_i$, $\hat{P}_{ij} = 3/2\ (\hat{S}_i\hat{S}_j+\hat{S}_j\hat{S}_i) - 2\delta_{ij}$, $i,j=x,y,z.$

The S_i are 3x3 pauli spin matrices. Using the definition

$$\langle O_i \rangle = \text{tr } \rho O_i / \text{tr } \rho \ ,$$

the expectation value for the vector polarization operator $\hat{P}_z$ is

$$P_z = \langle \hat{P}_z \rangle = \frac{N_+ - N_-}{N_+ + N_- + N_0} \ .$$

P_{zz} is the expectation value for spin alignment in the z direction,

$$P_{zz} = \langle 3\hat{S}_z^{\,2} - 2 \rangle = \frac{N_+ + N_- - 2N_0}{N_+ + N_- + N_0} \ .$$

$P_{zz}=+1$ when $N_0=0$, and $P_{zz}=-2$ when the beam has no alignment along the z axis ($N_+=N_-=0$).

Now, when the spin-orbit effects and nucleon spins are ignored in deuteron-proton scattering, the multiple scattering theory predicts no vector polarization and no off-diagonal alignment, leaving only three non-zero terms in the density matrix expansion:

$$\rho = \frac{\text{tr } \rho}{3} \left(1 + 1/2\ P_{zz}\hat{P}_{zz} + 1/6\ (P_{xx}-P_{yy})(\hat{P}_{xx}-\hat{P}_{yy}) \right)$$

with $\hat{x},\hat{y},\hat{z}$ along the principle axes of the scatter $\hat{q},\hat{n},\hat{k}$. The spin alignment in the secondary beam can be specified in terms of only two alignment parameters.

The double scattering cross section is

$$d\sigma/d\Omega\,|_{a,b} = \frac{3}{\text{tr } \rho_a}\ \text{tr } \rho_a \rho_b \ ,$$

with a and b representing the first and second scatters and $\rho=1/3\ MM^{\dagger}$. Now, we may expand ρ_a as above with $(x,y,z)=(\hat{q}_a,\hat{n}_a,\hat{k}_a)$. If we expand ρ_b in a similar way, the operators $\hat{P}_{zz}(b)$ and $\hat{P}_{xx}(b)-\hat{P}_{yy}(b)$ must have different spatial orientations from those of ρ_a, since $\hat{q}_a \neq \hat{q}_b$ and $\hat{k}_a \neq \hat{k}_b$. The general transformation from one set of operators into the other is somewhat complicated. If we take $\hat{k}_a=\hat{k}_b$ (this is small angle scattering, so the approximation is a good one), then

$$\hat{P}_{zz}(b) = \hat{P}_{zz}(a)$$

$$(\hat{P}_{xx}(b)-\hat{P}_{yy}(b)) = (\hat{P}_{xx}(a)-\hat{P}_{yy}(a))\cos 2\varphi$$

where phi is the azimuthal angle of the second scatter,

$$\varphi = (\hat{q}_b,\hat{q}_a) \quad .$$

The double scattering cross section becomes

$$I_{a,b} = I_{0b}\ (1 + a_1 b_1 + a_2 b_2 \cos 2\varphi)$$

with I_{0b} the second scatter unpolarized cross section, the a_i alignment parameters for the first scatter, and b_i the alignment parameters for the second scatter. For scattering at the same angles, the a_i equal the b_i. Specifically,

$$a_1 = 1/\sqrt{2}\ P_{zz}(t_a) = 1/\sqrt{2}\ \frac{2a_{11}-2a_{00}}{2a_{11}+a_{00}}$$

$$a_2 = 1/\sqrt{6}(P_{xx}(t_a)-P_{yy}(t_a)) = 1/\sqrt{6}\ \frac{6a_{1-1}}{2a_{11}+a_{00}}$$

$$I_{0b} = 1/3\ (2b_{11}+b_{00})$$

where $\rho_{ij}(t_a) \overset{d}{=} a_{ij}$, $\rho_{ij}(t_b) \overset{d}{=} b_{ij}$.

The term $(1+a_1b_1)$ adds a dependence on the first scatter to the second scatter cross section. The $\cos 2\varphi$ asymmetry is

$$A = \frac{a_2 b_2}{1 + a_1 b_1}$$

C. Predictions

The multiple scattering theory predicts very large asymmetry for optimum scattering angles in deuteron-proton scattering. In terms of the spherical and quadrupole scattering amplitudes,

$$a_1(t)=b_1(t)=\sqrt{2}\,\frac{-3/4\,|Q|^2 + 9/4\,|Q1|^2 + 3\mathrm{Re}\,M^{\dagger}Q}{3|M|^2 + 3/2\,|Q|^2 + 9/2\,|Q1|^2}$$

$$a_2(t)=b_2(t)=\frac{-3\sqrt{6}\,\mathrm{Re}(M^{\dagger} + 1/2\,Q^{\dagger})Q1}{3|M|^2 + 3/2\,|Q|^2 + 9/2\,|Q1|^2}$$

The imaginary parts of M, Q, and Q1 were given in Figure 3. Figure 4 shows the alignment parameters and Figure 5 shows the resulting cross section and asymmetry prediction versus the first scatter four momentum transfer-squared, with the analyzer set at our experimental value of $-t_b = .23\ \mathrm{Gev}^2/c^2$.

Returning to Figure 3 and the expression for the alignment (a_2) above, the characteristics of the asymmetry are surprisingly independent of the amount of D-wave present. Maximum alignment occurs near the angle where Im Q = Im M , giving

$$a_2 \cong b_2 = -\sqrt{6}/2$$

$$a_1 \cong b_1 = 1/\sqrt{2} \quad .$$

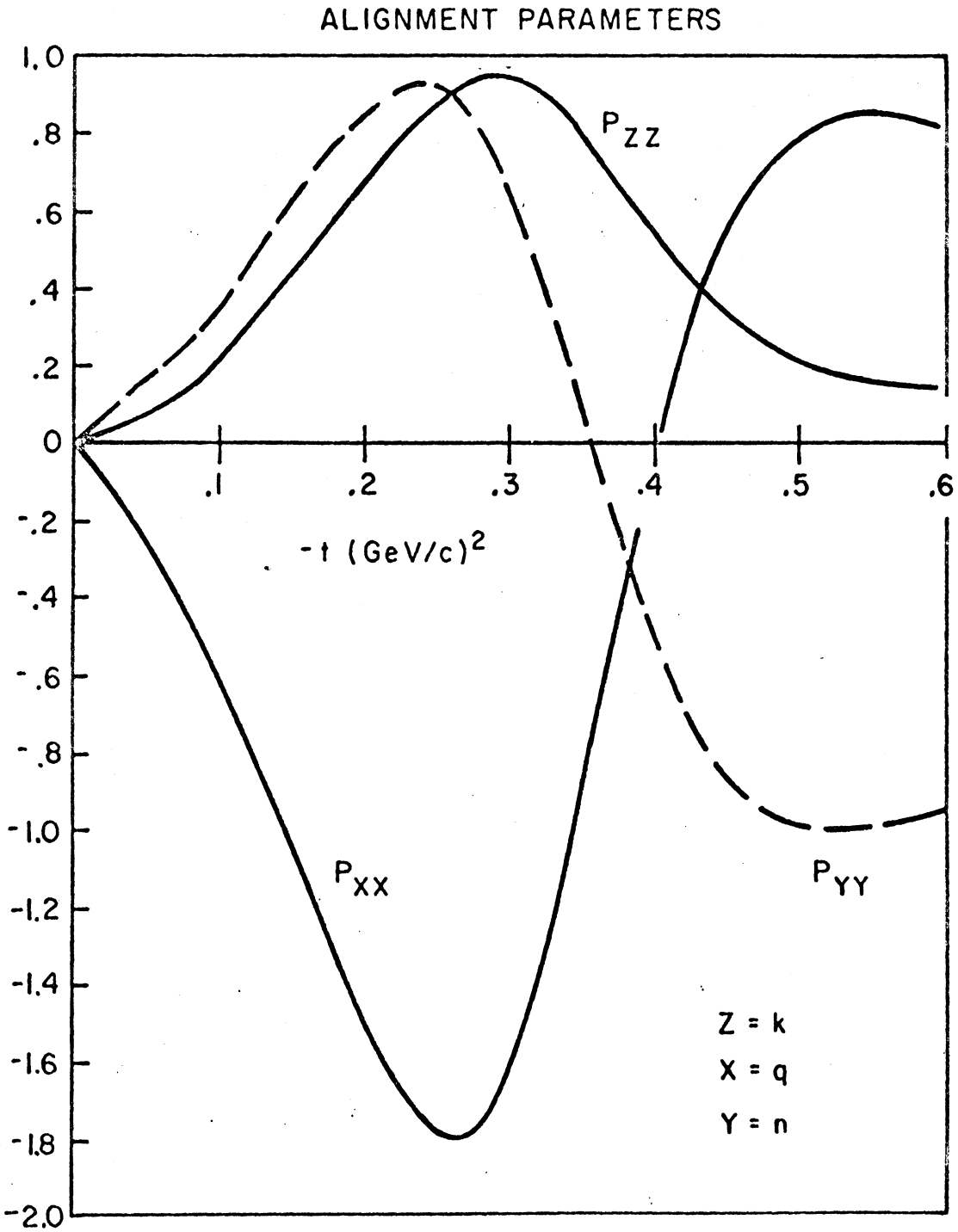

Figure 4. The alignment parameters for d-p scattering, calculated by the multiple scattering model.

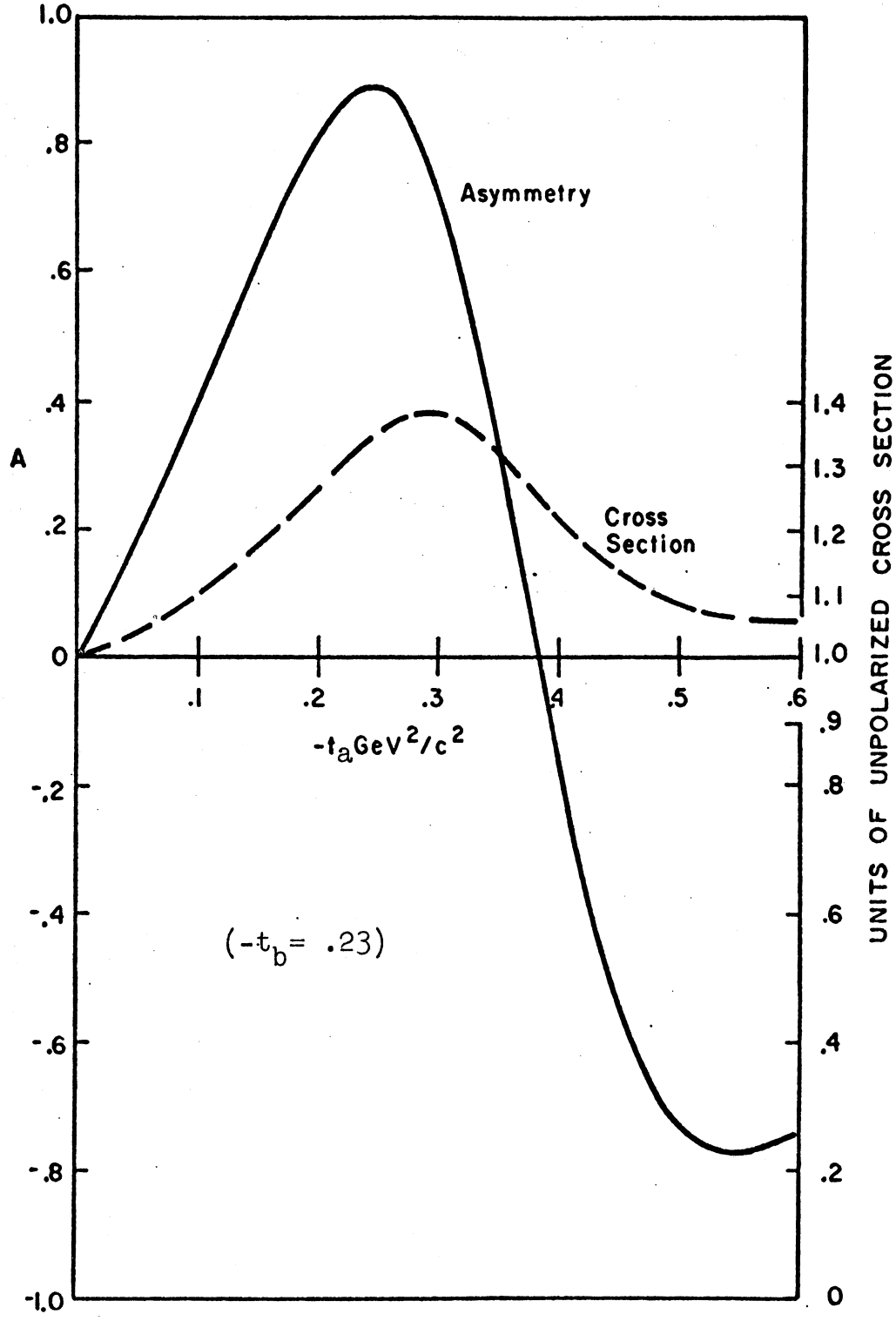

Figure 5. Double scattering predictions from the Glauber model. For $I = I_0 (1 + a_1 b_1 + a_2 b_2 \cos 2\varphi)$,

$$\text{Asymmetry} = \frac{a_2 b_2}{1 + a_1 b_1} \quad , \quad \text{Cross section} = I_0 (1 + a_1 b_1) .$$

The $\cos 2\varphi$ asymmetry, then, is $A = +1$. Thus, total alignment occurs only because the spherical and quadrupole amplitudes cross. The size of the effect is not very sensitive to the D-wave probability. It is considerably more sensitive to the real parts of the nucleon scattering amplitudes.

The multiple scattering theory predicts total $z = k$ alignment at $-t = .27$ Gev$^2/c^2$, along with total $y = n$ alignment. No spins should lie along the $x = q$ axis. Note that for small $|t|$, $P_{zz} = P_{yy}$. This is due to the domination of the single scattering term, where the n and k directions are equivalent[20] (see page 11).

Later, we will compare the theory both to our polarization data and to the pd unpolarized forward cross section results at 1 Gev. In terms of the monopole and quadrupole scattering amplitudes, the cross section is

$$d\sigma/d\Omega\,|_{lab} = |M|^2 + 1/2\,|Q|^2 + 3/2\,|Q1|^2$$

III. THE APPARATUS

A schematic diagram of the beam line at the Princeton-Pennsylvania Accelerator is in Figure 6 (also Figure 2). The deuteron beam from the synchrotron of 10^{12}/second was scattered by a ten inch hydrogen target at position T1. A secondary beam of elastic deuterons was defined and focused by a combination of slits, bending magnets, and quadrupoles and was scattered off the hydrogen target at T2. A range analyzer wrapped around the target at T2 determined a momentum transfer interval for the recoil proton in the second scatter and counters downstream detected elastically scattered deuterons at this momentum transfer, along with a broad range of background. The trajectory of the forward particle was determined by the four wire chamber planes.

A. The First Scatter

The first hydrogen target bag was $1\frac{1}{2}$" diameter, 10" long. Scattering of the 10^{12}/second deuteron beam gave about 10^4 elastic deuterons in the secondary beam. Figure 7 shows the dimensions involved. The magnet-slit system defined a four momentum transfer-squared range of

$$dt_a = .01 \text{ Gev}^2/c^2$$

with a quite pure secondary beam (almost all the reaction products of a deuteron beam are at half the momentum of the elastic deuterons or less). An example of a magnet curve run by sweeping D1, with D2 and D3 off, and the

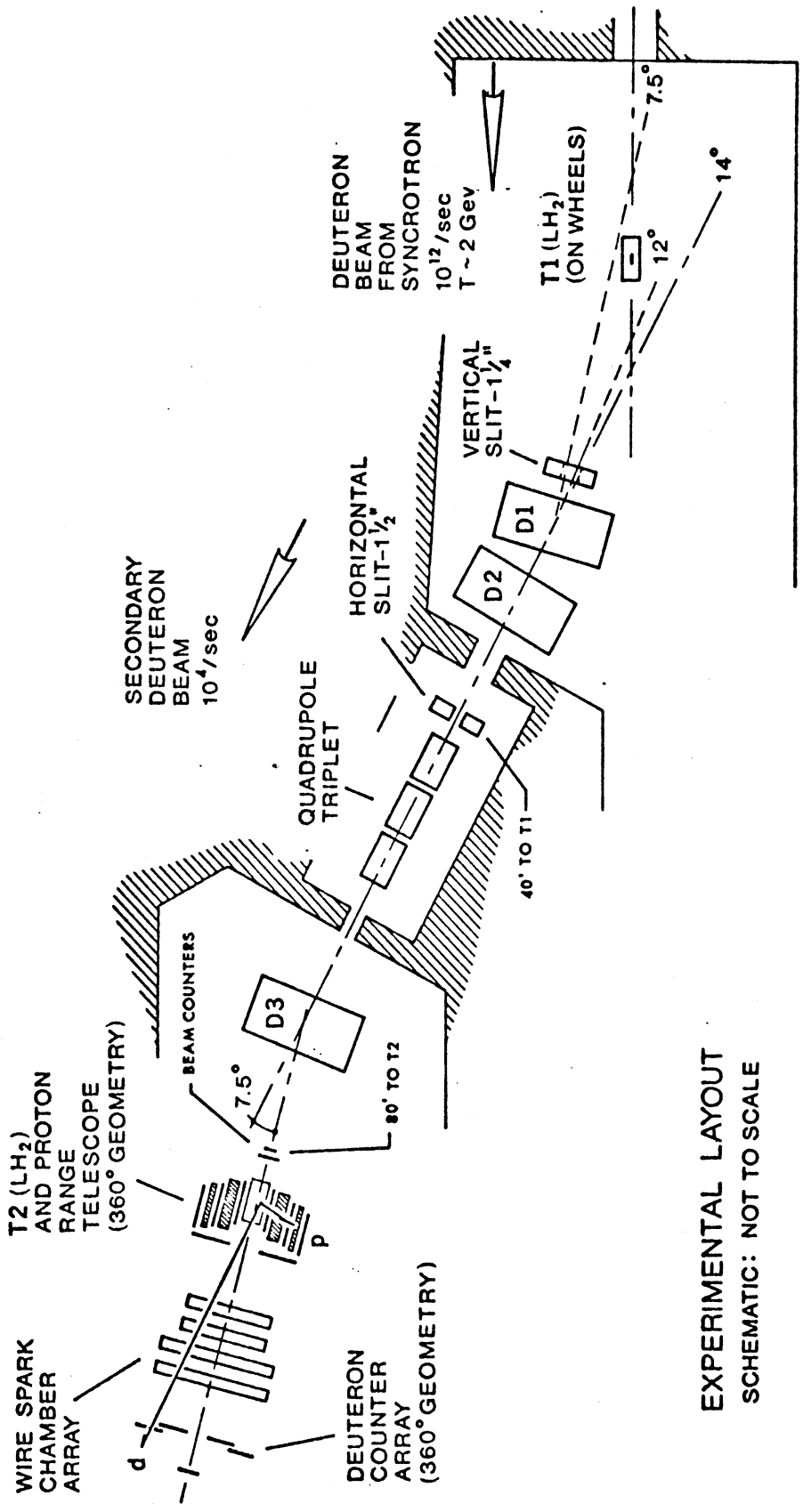

Figure 6. Schematic of experimental area (also Figure 2).

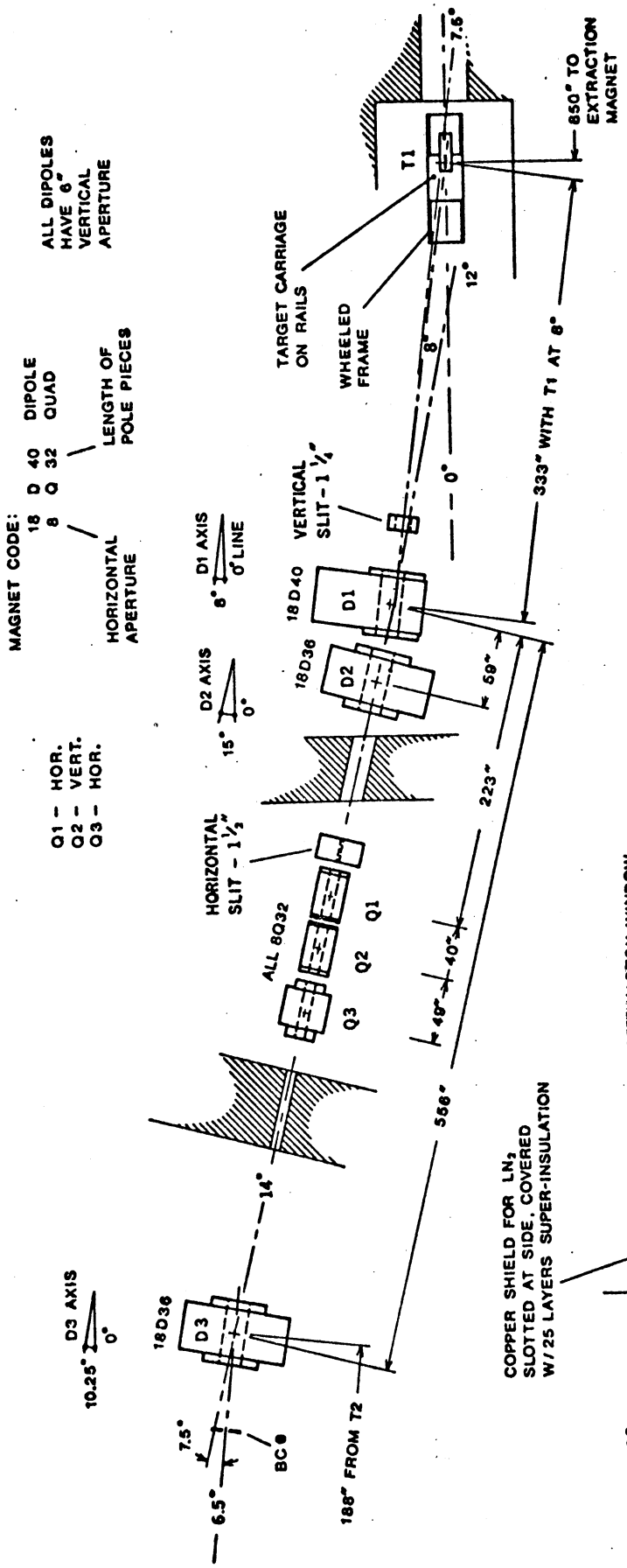

Figure 7. Dimensions of first scatter area and secondary beam line.

quadrupoles scaled accordingly is in Figure 8. (BC1 is a 1" counter centered on the undeflected beam line near the second target.) The beam intensity dropped by a factor of twenty for target empty runs.

Three techniques were used to vary the first scatter momentum transfer. We used four different incident beam energies (most at 3.57 Gev/c), we moved the target along the beam line to define scattering angles from 7.5 degrees to 12 degrees, and we interchanged dipoles D1 and D2 for the first bending magnet. Thus, we covered

$$-t_a = .13 \text{ to } .54 \text{ Gev}^2/c^2 .$$

The beam momentum varied by 3% over the 3 msec extraction time of the synchrotron (the spill time). This energy variation was time correlated with the beginning of the spill and by recording on magnetic tape the time of each event in the spill, the incident momentum was known to less than 1%. Without using the timing information, the first scatter window would be $dt_a = .03 \text{ Gev}^2/c^2$. The incident beam position was monitored by television cameras looking at scintilators along the beam line. The incident beam spot size was about $\frac{1}{2}$" diameter and the beam dispersion was less than 5 mrad. We monitored the relative incident beam intensity with three well-shielded counters looking at a berylium target far downstream from the first target.

The vertical and horizontal slits kept the beam divergence to within $\pm$ 1/4 degrees and forced the

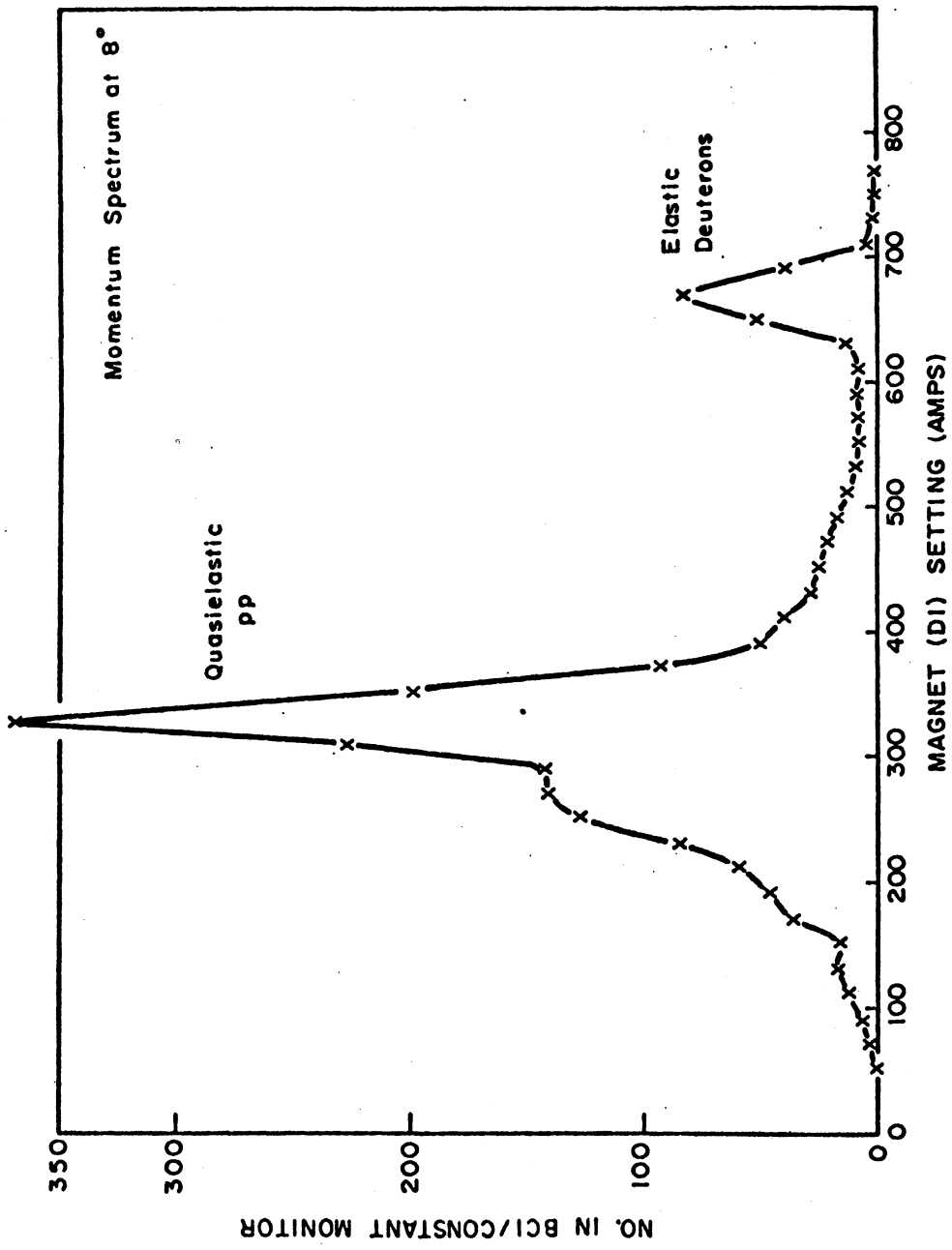

Figure 8. Secondary beam spectrum.

horizontal and vertical divergences to be roughly the same. This is important, since strongly different horizontal and vertical divergences can cause the same type of up-right asymmetry as that being measured. We took beam tracks through the spark chambers at the beginning of each run, both to monitor the beam divergences and to set a physical coordinate system for the second scatter.

The opposite bending angles of D1-D2 and D3 resulted in momentum recombination, allowing the scatters of varying incident beam energy to reach the second target. Thus, the combination of dipoles, slits, and quadrupoles defined the momentum loosely (to 10%) and the scattering angle closely (to $\frac{1}{2}$ degree), giving a quite pure secondary beam of elastic deuterons (Figure 8).

B. The Second Scatter

The second hydrogen target bag was 4" diameter by 15" long with an effective length of 10" due to the size of the recoil proton counters. The secondary beam was confined to a 2" diameter by counters BC2, BC3 (Figure 9). The momentum transfer of the second scatter was defined by the range of the wide angle (70 degrees) recoil proton in polyethylene. An accepted recoil particle (125 $\pm$ 8 Mev for protons) along with a forward particle in the proper quadrant triggered the four wire chamber planes. For a 10^4/second secondary beam, there were about two triggers per second. One twentieth of those were elastic events.

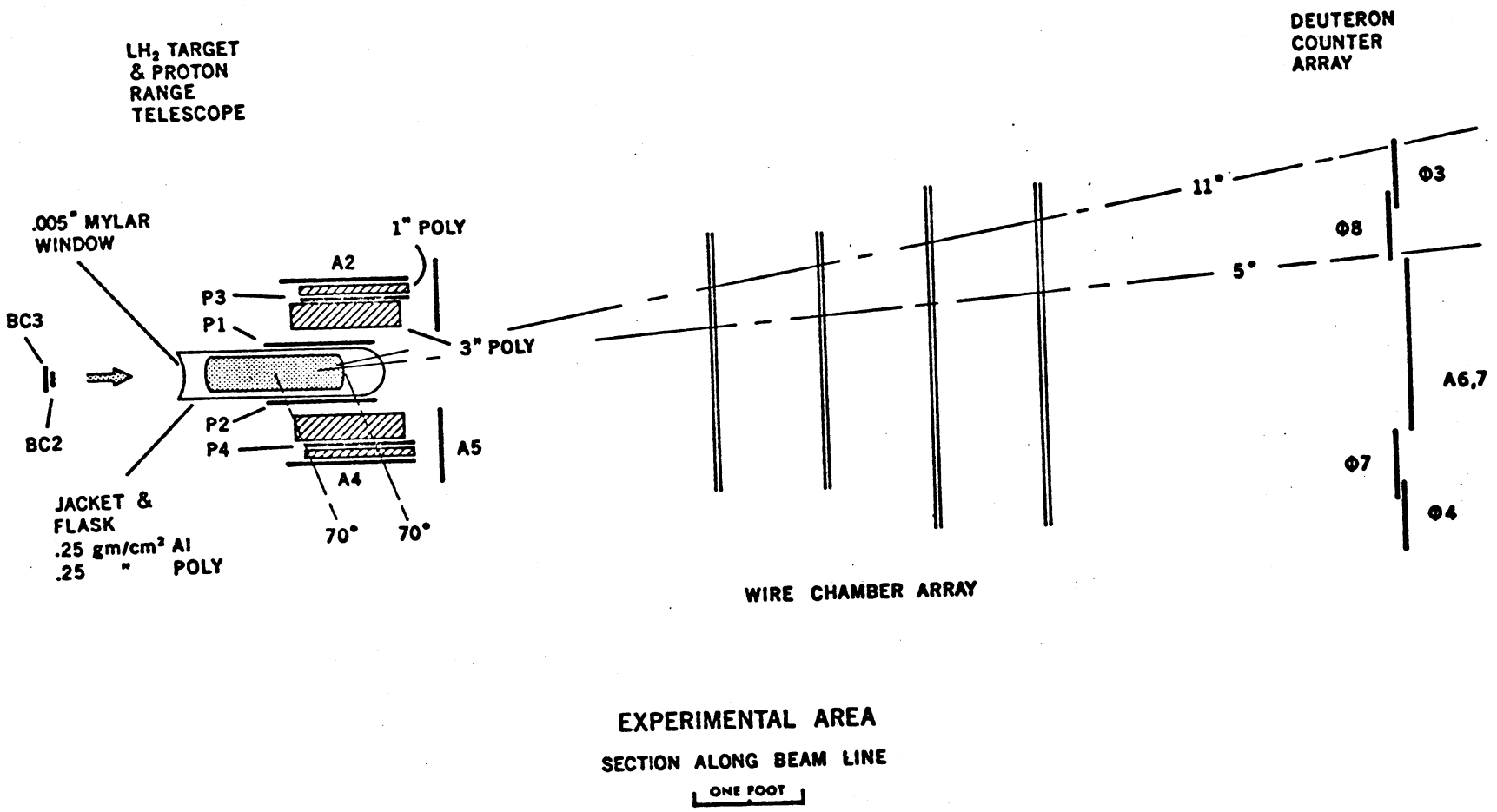

Figure 9. The second target area.

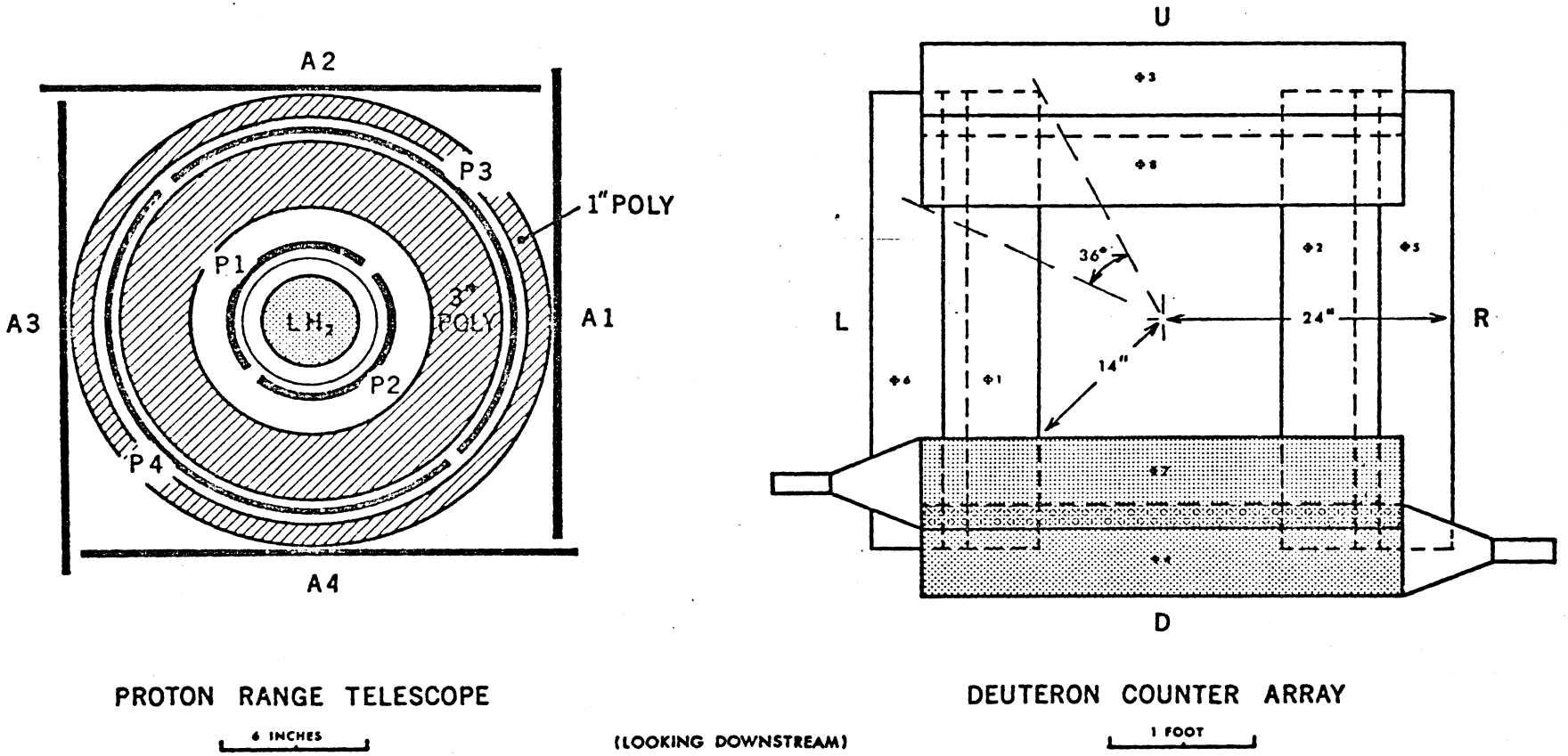

Figure 10. The proton range telescope and deuteron counter array.

The proton range telescope (Figure 10) consisted of four semicylindrical counters forming a sandwich around a three inch ring of polyethylene, a one inch polyethylene window outside of this, and five counters in anti-coincidence surrounding the wrap. A good recoil proton passed through the 3" absorber and came to rest in the 1" polyethylene window. The semicylinder proton counters were arranged to form four quadrants (up, down, right, left), with each semicylinder covering two quadrants. This method allowed us to monitor the possible asymmetries in the apparatus (the number up should equal the number down, for example) and also afforded a loose coplanarity check. We had the option of inserting various materials into the range wrap, increasing the amount of initial absorber, but we found the best analyzing power had no extra materials in the wrap.

Eight 8" x 40" x 1/4" counters called the phi counters, set in a square array downstream of the wire chambers, defined forward scattering angles from 4 degrees to 14 degrees. Arranged in quadrants, the deuteron counter array gave a loose coplanarity check in combination with the proton counters, and also gave a direct determination of the number of triggers up, down, right, left (Figure 10).

A coincidence between the proper combination of phi counter quadrant and recoil proton quadrant, and a beam

counter coincidence triggered the four wire chambers. In addition to the five anti-counters enclosing the target (the fifth, A5, is centered on the beam line with a 9" hole--see Figure 9), two other counters in anti-coincidence were in the hole of the phi counters on the beam line (Figure 9). These cut the trigger rate by 20%. Also, the three "spectator" proton quadrants were in anti-coincidence. The wire chamber planes then gave the trajectory of the forward particle.

C. The Trigger Logic

A diagram of the trigger logic is in Figure 11. Briefly,

$$BC2 \quad BC3 \quad \overline{BC0}$$

indicated a beam particle (BC9 had a 6" diameter hole through it--it removed half momentum protons from the trigger that were swept toward the left side of our apparatus by D3 (Figure 7).), while

$$P1 \quad P3 \quad \overline{P2} \quad \overline{P4} \quad \overline{A}$$

gave a recoil particle (up) with the proper range, and

$$\varphi 4 \cdot \varphi 7$$

determined a forward particle (down). The combination above triggered the spark chambers, with the read-out from the chambers going to scalers and then to a PDP-8 computer used to record the events on magnetic tape.

The process of taping takes tens of milliseconds, while the trigger logic time delay is on the order of

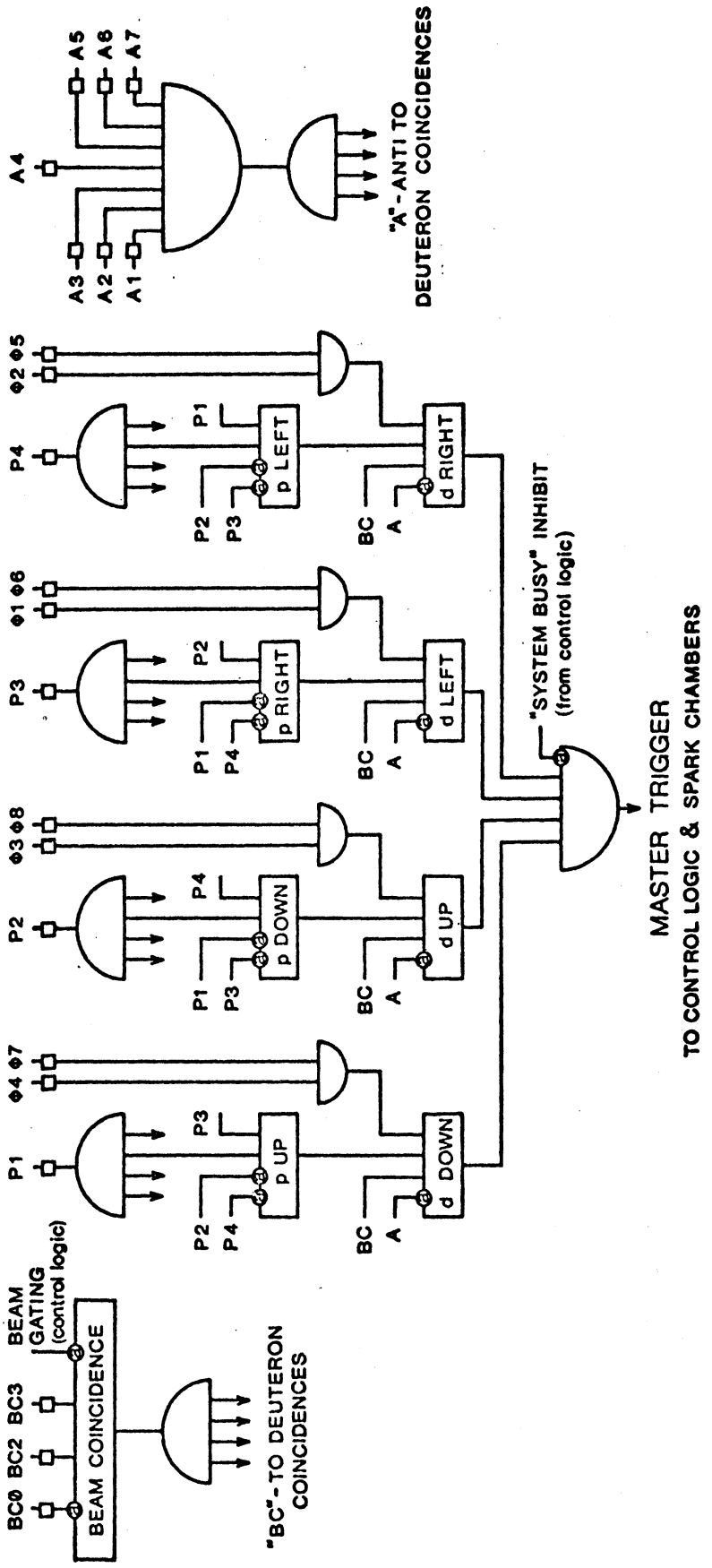

Figure 11. The trigger logic.

nanoseconds. A control logic system gated out the trigger logic during the processing of an event. The control logic freed the computer interface for recording when the computer and the chambers were in a ready state and the time during the spill was within specified limits.

Several items not in the trigger logic should be mentioned. Time-of-flight was taken on the secondary beam, but no contamination was seen, so it was removed from the logic (over the eighty foot path length involved, a pion travelling at speed c would arrive at the target 12 nsec earlier than the elastic deuteron with β=.87). A hodoscope placed between the quadrupoles and D3 was used to monitor the beam early in the experiment, but it had little effect in the trigger and was removed. A helium bag ran the full distance of the secondary beam line, reducing stripping and other interactions there. Magnet tuning was done by first turning off D3 and optimizing the beam on counter BC1 in the undeflected beam line, then swinging the beam onto BC2-BC3. The magnet fields (determined by accelerator graphs and checked by a rotating coil gaussmeter to 1%) checked with the experimental geometry and kinematics quite well.

D. The Spark Chambers and Read-out

The four wire chambers were spaced each one foot apart. The active areas were 30" x 30" for the front two chambers and 40" x 40" for the back two, with

1 mm wire spacing and a $\frac{1}{2}$" gap. Receipt of a trigger from the high speed logic activated three spark-gaps, firing the chambers and the fiducials. The front pair were run at about 9 kV, the back two at 8 kV. The chambers were covered by aluminum foil, and a 250 V clearing field across the foil planes resulted in a live time of about one microsecond. The chambers were filled with a 90% neon, 10% helium gas mixture. Two spark-gaps fired the chambers, while the third fired the fiducials. Data were taken with a single fiducial on each dimension, while double (front-back) fiducial runs were made periodically to determine the scaling factor for the read-out.

Dynamic magnetostrictive wands were used to read the spark information out of the chambers. Each wand was read with a 15 MHz scalar. Missing or multiple sparks caused nonsense scalar outputs. The signal attenuated by two thirds over a 42" wand, but the smallest signal was easily recognized by the scalars, so no asymmetries were introduced here. This was checked by reversing three wands for several runs. Results from the scalars were strobed by a PDP-8 computer, which stored the numbers, writing ten events per record on magnetic tape. Information on each event consisted of the eight wand read-outs (integers) plus a number representing the time of the event in the spill (the spill time of 3. msec was divided into 400 bins).

The computer made no checks on the data--it was used only for writing on tape and to display selected events on a teletype.

E. Data Taking

Each run, consisting of a particular first target setting and beam momentum, took from a few hours for low momentum transfers to a full day for high momentum transfers. Over a three week period, we gathered data for different first target settings and for four different beam momenta, repeating several points. There were 31 runs in all with 7000 to 42000 events each, covering sixteen first scatter momentum transfer values. Only two of the runs processed poorly (both showed chamber difficulties). About 5% of the triggers represented elastic events.

The runs were prefixed with 1000 beam tracks (the chambers triggered on BC2 BC3 $\overline{BC0}$) and 1000 "real space" tracks (triggering on a 3/8" counter fixed in space in the secondary beam line far downstream from the second target). The beam tracks for each run located the coordinate system for event reduction, while the real space tracks were taken for possible phase space uses, but were not needed.

During each run, the beam counts, the number of triggers in the four quadrants, and the counts in each of the four proton quadrants and the four phi quadrants

were recorded in the log book for each run, along with a rate record from an independent primary beam monitor on the unscattered beam line.

IV. DATA ANALYSIS

A. Data Reduction

Data reduction took place off line on the accelerator's PDP-10 computer during the experiment. The computer program used the 1000 beam tracks to locate a coordinate system and made chi-squared fits to the data for all four chambers and for combinations of three chambers. A good event had an acceptable chi-squared fit in at least three chambers and reconstructed back to the target. The chamber fits indicated an uncertainty of about $1\frac{1}{2}$ wire separations, twice that seen in the double fiducial tracks. Most of the error probably resulted from sparking phenomena. The resulting average angular uncertainty for a three chamber fit is only .03 degrees.

Fiducials and chamber center corrections were used in the analysis. Chamber cuts (removing one chamber from the analysis; requiring a four chamber fit) produced inconsistencies in only two of the runs, and these were thrown out. The chamber efficiency varied during the runs from 40% to 70%, with most about 60%.

For the final data, runs taken at the same energy and momentum transfer were combined, giving eighteen data points.

B. Background Discussion

Figure 12 shows a typical histogram in the scattering angle theta for one of the runs. About half the triggers under the elastic peak are background. Phi distributions for triggers within the elastic peak (the raw data) are given in Figure 13 for one of the high positive asymmetry runs and for a negative asymmetry run. There was a strong signal despite the background. With no background subtractions, we obtained an asymmetry versus first scatter momentum transfer curve very similar to the final result, but with a maximum asymmetry of .45 instead of .67.

We can only speculate on the nature of the background. Quasielastic pp scattering was probably the major contributor. Pure quasielastic pp scattering yields a proton at 16 degrees for a given recoil proton range, while the spectator proton from np scattering peaks at 0 degrees. The Fermi momentum of the nucleons in the deuteron contribute to considerable broadening about these peaks, and also make the quasielastic scattering less coplanar (more quasi). The 8 degree elastic deuteron peak probably sat on the tails of the quasielastic and spectator peaks.

There were indications that particle production was involved in the background. The use of anti-counters on the beam line cut the trigger rate by 20%, indicating

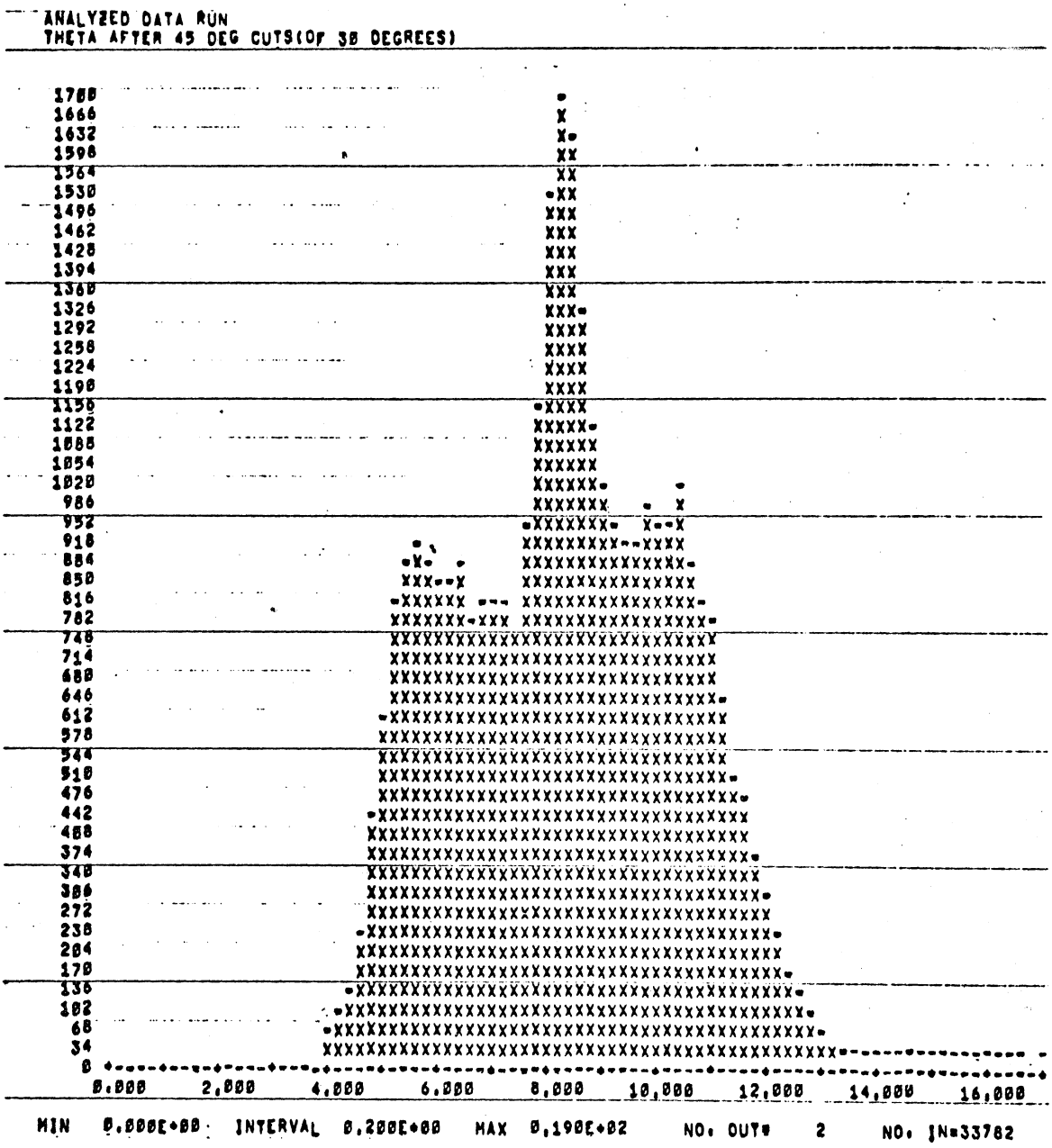

Figure 12. Theta histogram of raw data.

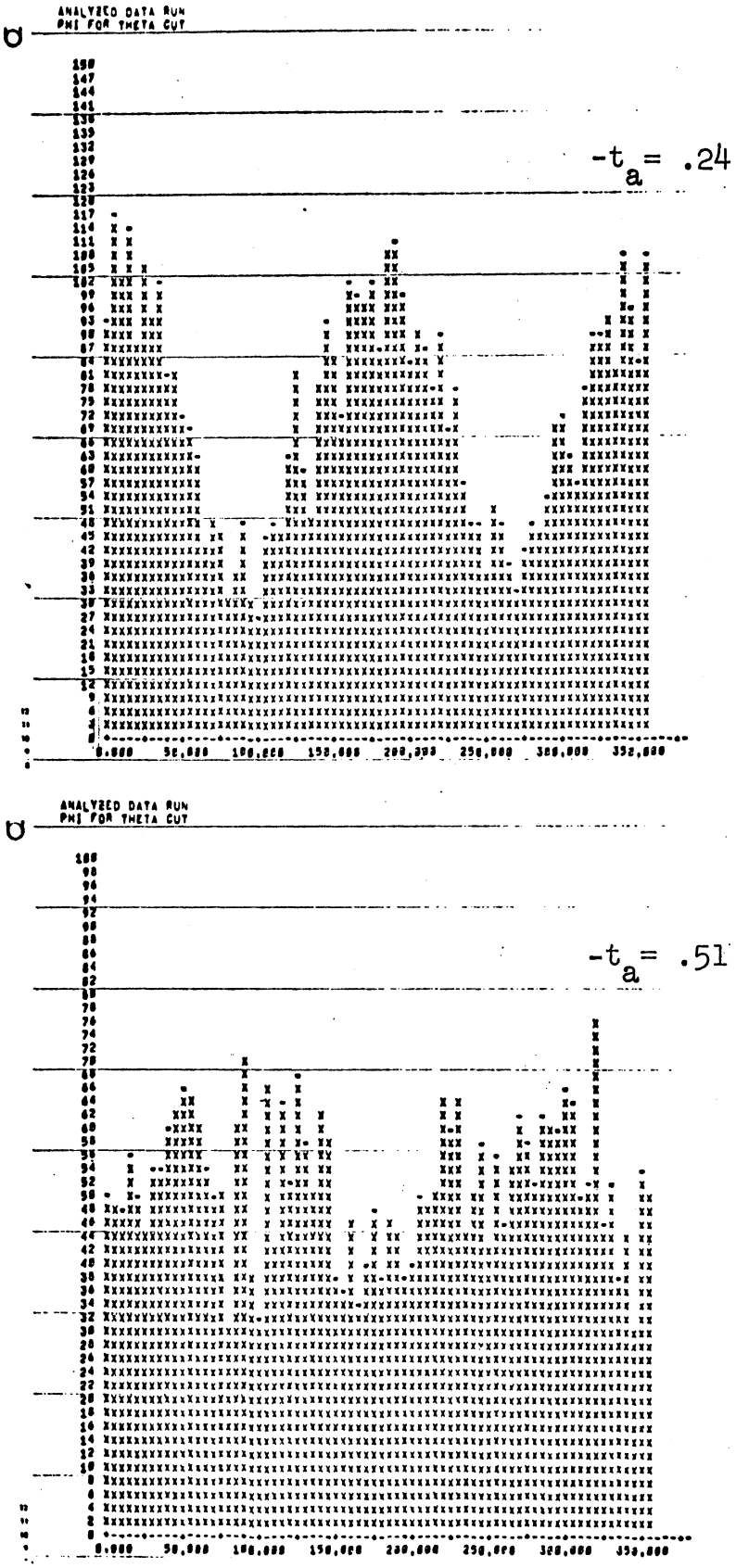

Figure 13. Phi histograms of raw data.

a process such as

$$np \rightarrow pp\pi^-$$

must have contributed, with the spectator proton proceeding downstream to the anti-counters . Lowering the incident beam energy (from 3.57 Gev/c to 2.6 Gev/c) gained a factor of about 20% on the background. This is in the range of an exponential increase in the total cross section for pion production[21]. Finally, a run triggering only on protons up, anded with each of the phi counter quadrants, gave one fourth the triggers in each of the three non-coplanar quadrants as the number in the coplanar quadrant. Thus, the background did not seem to be very coplanar.

C. Background Subtractions

Several points should be made before we describe the background cuts. First, the raw data showed strong asymmetry over the elastic peak with reasonable least-squared fits to

$$N(\varphi) = N\ (1 + A\cos 2\varphi + B\cos\varphi)\ .$$

The $\cos 2\varphi$ or up-right asymmetry dropped off and the chi-squared generally became much worse in non-elastic regions of scattering angle. The $\cos\varphi$ or right-left asymmetry was negative ($B \cong -.10$) on both sides of the elastic peak, was generally zero for the data under the peak, and was relatively independent of the first scatter momentum transfer. Phase space corrections were not necessary, due to the 360 degree geometry of the apparatus,

and the oversized phi counters which easily contained the whole elastic region. Finally, an overlap of the phi counter quadrants in the 45 degree areas caused a building of background there, so 30 degree sections of data about the four 45 degree lines were ignored.

In making the background subtractions, we allowed for possible background asymmetries and a variable secondary beam dispersion. The data for each run were divided into twelve 20 degree sections in phi; we fit the theta distributions of the total data and the twelve phi sections with a gaussian representing the elastic peak and a sloped line for the background. An example of fits for the four quadrants of a high asymmetry run is given in Figure 14. The fit to the total data for each run was free of constraints, but the fits to the twelve sections were required to be centered within .2 degrees of the center for the total curve and the width of the gaussians were kept within .15 degrees of the width of the total curve. Background subtractions then gave a twelve point phi distribution (Figure 15).

We made several checks on the computer subtractions. The fits were required to look reasonable. Agreement between the twelve point fits and fits to four 60 degree sections was checked. Integrals over the elastic peak, summed over the twelve sections, checked with the fit to the total and with the fits to the quarters. The integral over the gaussian agreed with the sum of the "real" deuterons in the elastic peak. Different binning

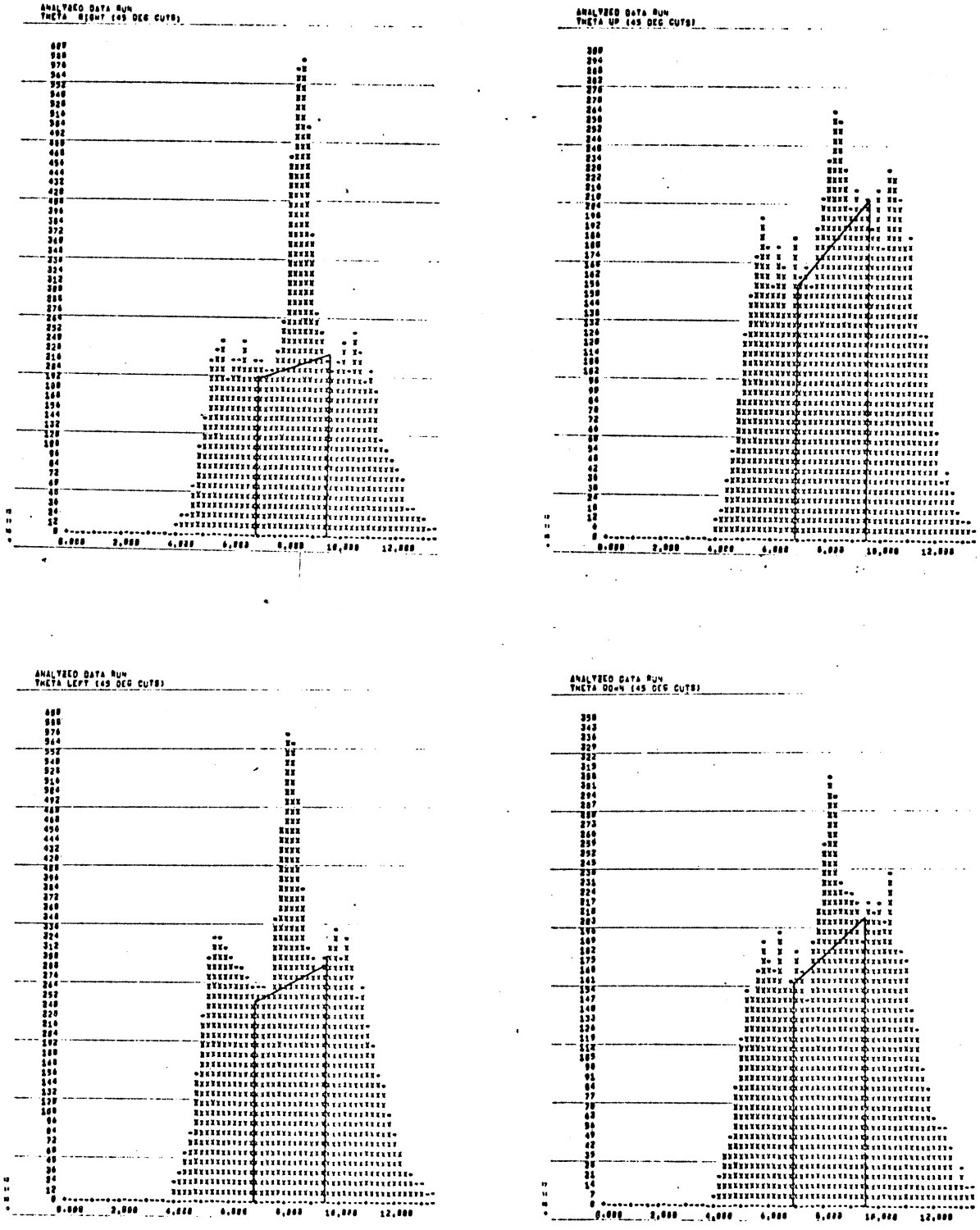

Figure 14. Example of Background Subtraction.

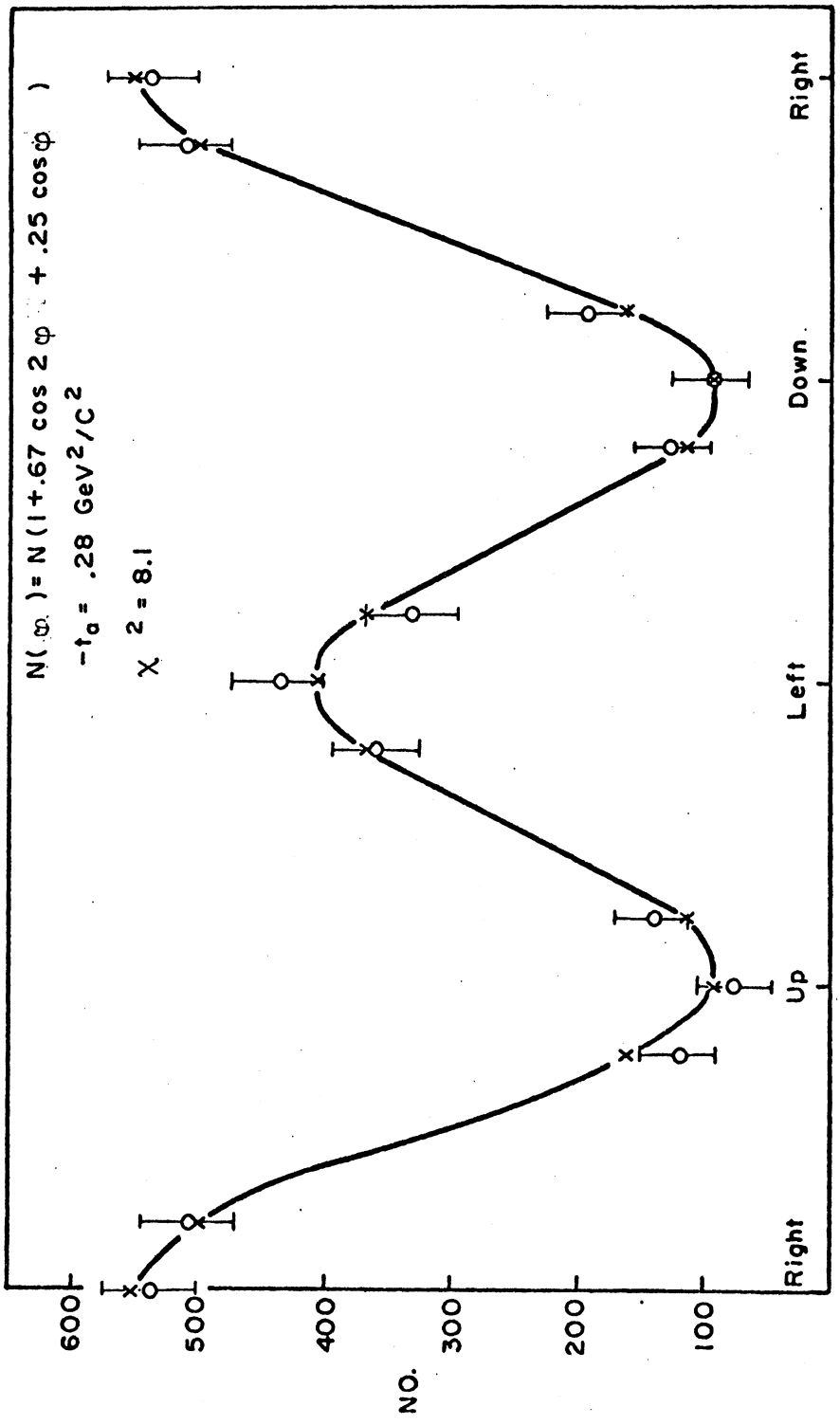

Figure 15. Twelve point phi distribution after background subtraction for a high asymmetry run.

in theta (fitting over a 3.6 degree interval compared to a 4.6 degree interval) gave consistent results. Eyeball fits assuming bumps or dips in the background under the peak were tried. These tended to leave the up-right asymmetry in tact, changing the right-left asymmetry some for individual runs, but left the overall right-left asymmetry curve the same.

V. RESULTS

Table 2 gives the results, after background subtractions, for the $\cos 2\varphi$, $\cos\varphi$, and $\sin\varphi$ asymmetries in the elastic peak and in the background, along with the relative cross section for elastic scattering. The t_a value given is the average t_a for each run. Each t value has an uncertainty of $\pm$ .01 Gev^2/c^2, reflecting a systematic error due to a variation in peak beam energy of the accelerator from run to run. (The uncertainty due to the variation in beam energy over the spill is also within this range.) The elastic results are plotted versus first scatter momentum transfer-squared in Figures 16, 17, 18.

The shape of the $\cos 2\varphi$ asymmetry curve (Figure 16) is the same with or without background subtractions, the only change being increased magnitude. Whereas the background subtractions giving a maximum $\cos 2\varphi$ asymmetry of .67 look quite reasonable, a subtraction raising the asymmetry to .8 or .9 looks absurd. The solid line in the figure is the multiple scattering calculation for A, ignoring the target proton spin, with no free parameters.

The $\cos\varphi$ asymmetry (Figure 17) appears only after background subtractions. The relatively constant $\cos\varphi$ term of .25 is more dependent on the subtraction technique, but is present throughout the data. Scattering to the left consistently showed a smaller elastic peak sitting on a larger background than scattering to the right. The background right-left asymmetry is negative

	Elastic Fits								Background under peak			Raw Data	
-t	A	ΔA	B	ΔB	Ω	ΔΩ	C	N(K)	A	B	N(K)	A	B
.13[a]	.40	±.04	.16	±.06	.343	±.016	.07	1.45	.20	-.03	3.1	.26	-.00
.19[b]	.61	.04	.37	.06	.283	.014	-.02	1.45	.23	-.08	3.5	.39	.11
.23	.63	.06	.07	.10	.345	.028	.00	.58	.21	-.27	1.7	.37	-.05
.24	.66	.04	.32	.05	-	-	-.04	2.69	.16	-.07	7.2	.40	.11
.24[b]	.67	.03	.13	.06	.318	.014	-.09	1.80	.23	.02	4.2	.45	.04
.24[a]	.65	.06	-.03	.11	.401	.029	-.25	.54	.26	-.07	1.0	.38	.09
.25	.53	.05	.29	.07	.247	.013	-.10	1.55	.22	.07	4.1	.36	.07
.28	.67	.03	.25	.05	-	-	-.03	3.31	.22	-.11	9.6	.39	.02
.30	.54	.06	.23	.09	.268	.019	.00	.76	.09	-.09	2.0	.32	-.01
.32	.46	.04	.14	.06	.327	.013	-.00	2.02	.21	-.16	4.6	.37	-.01
.33[b]	.45	.05	.11	.07	.296	.016	-.02	1.25	.12	-.11	3.1	.23	-.01
.34	.29	.04	.26	.05	.314	.012	.04	2.53	.06	-.14	7.5	.20	.00
.38	.15	.06	.33	.08	.246	.016	-.06	.95	.06	-.05	2.9	.09	.12
.40	.08	.08	.54	.10	-	-	-.06	.55	.00	-.07	2.0	.07	.08
.43	-.14	.04	.23	.06	.403	.018	-.04	1.72	-.01	-.11	4.2	-.04	.05
.48	-.19	.04	.09	.05	-	-	.00	2.23	-.06	-.14	7.3	-.06	-.01
.51	-.26	.05	.18	.07	.250	.014	.00	1.03	-.06	-.06	2.4	-.11	.07
.54[c]	-.37	.11	-.18	.15	.236	.030	-.08	.22	-.04	.00	.6	-.14	-.05

a. 2.64 GeV/c b. 3.16 GeV/c c. 3.70 GeV/c

Table 2. Results. Fits are to $N(\varphi) = N/2\pi\ (1 + A\cos 2\varphi + B\cos\varphi + C\sin\varphi)$. Ω is the relative cross section, defined in the text. Primary beam momentum is 3.57 GeV/c , unless otherwise noted. Error in t is ± .01 $(GeV/c)^2$.

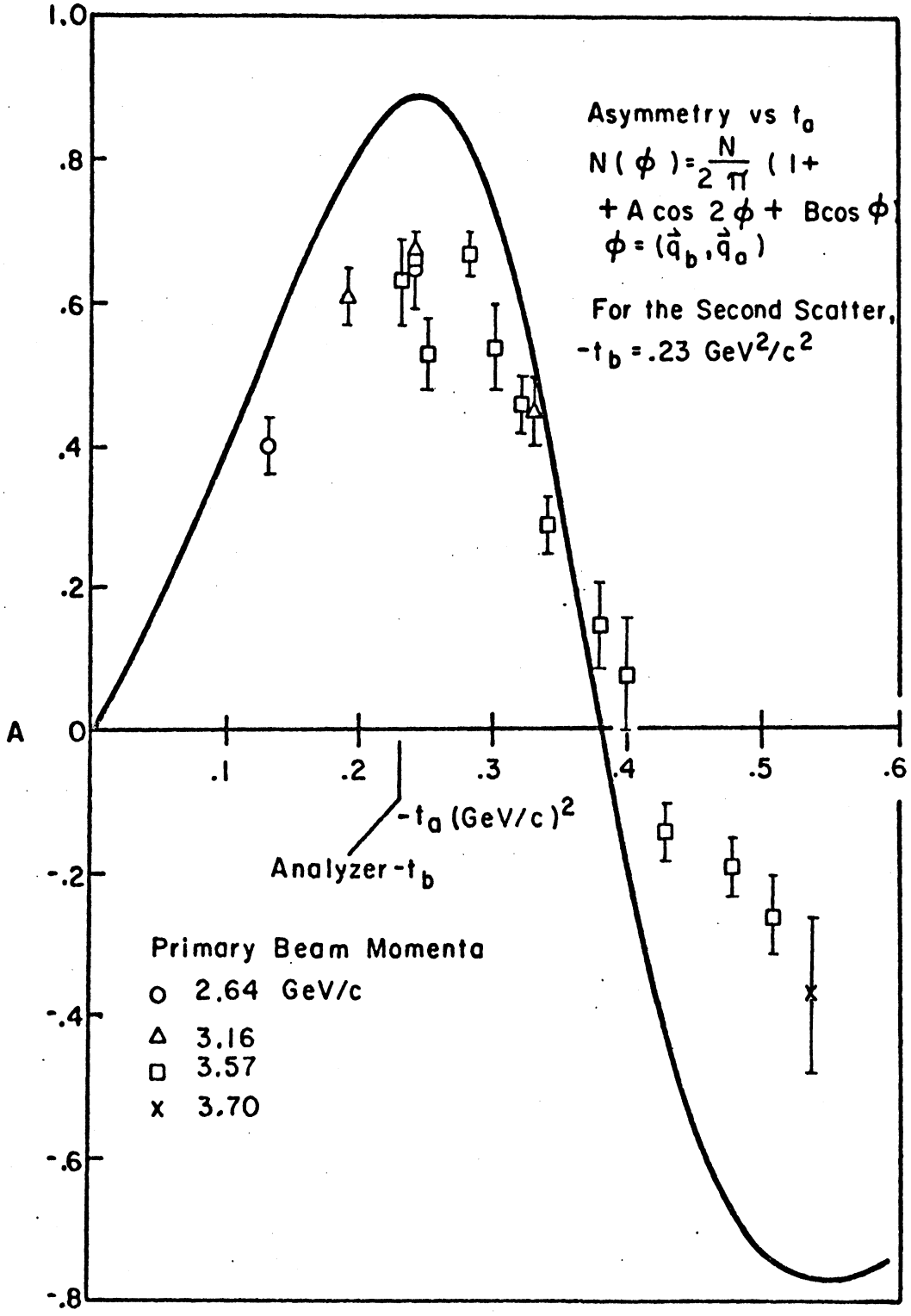

Figure 16. Cos2φ asymmetry data of Table 2, including the Glauber model fit with no free parameters.

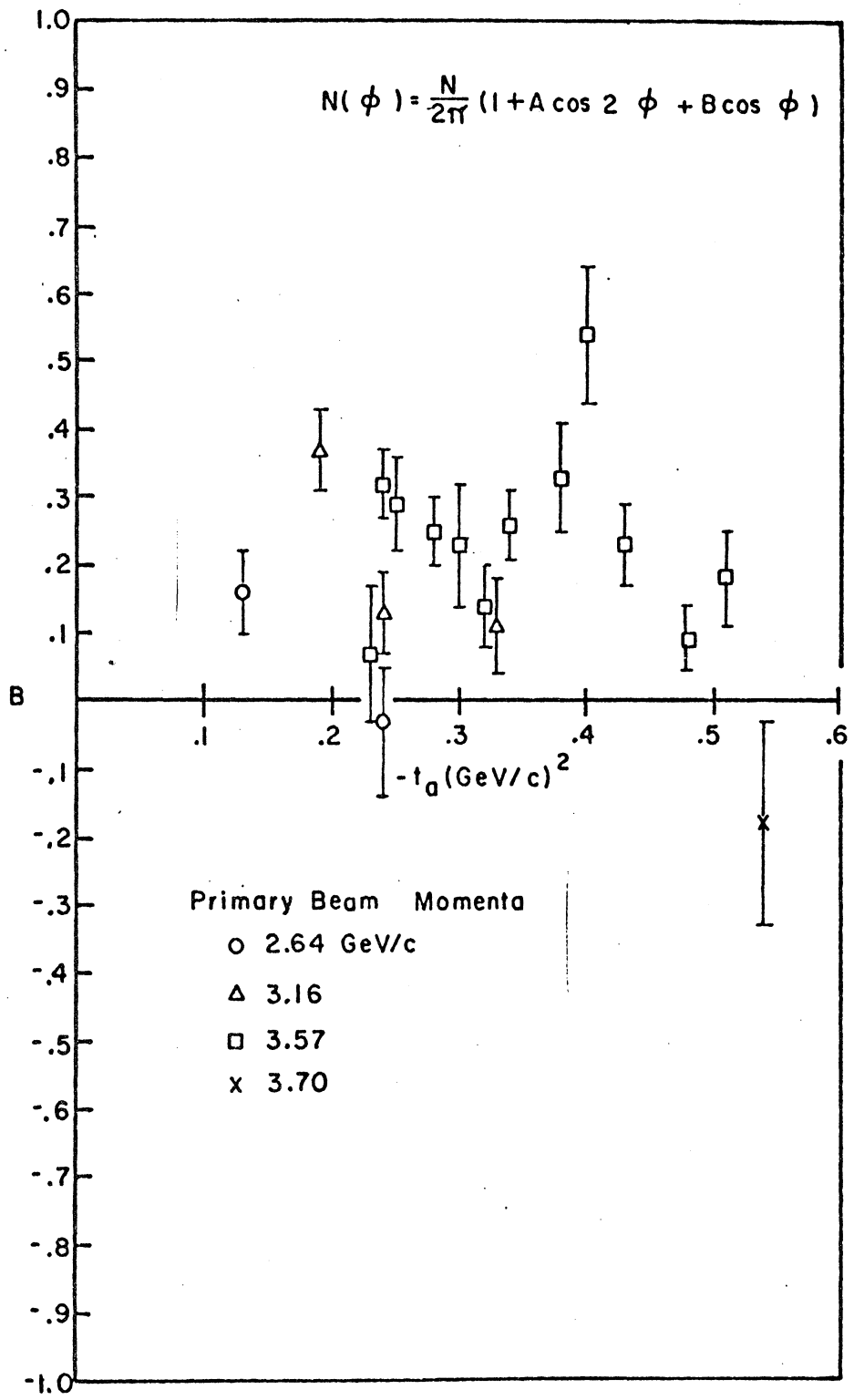

Figure 17. Cosφ asymmetry data of Table 2.

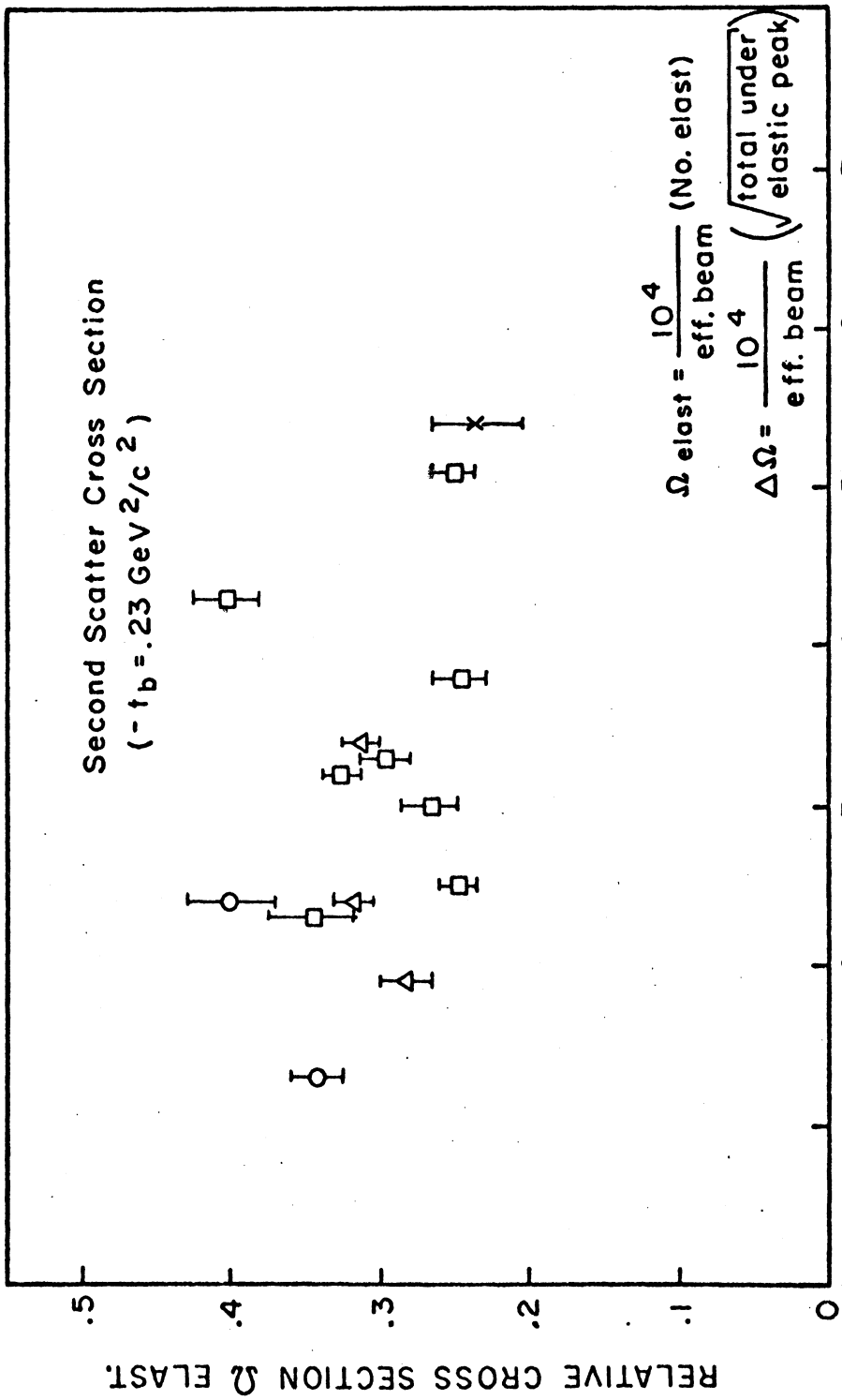

Figure 18. Relative second scatter cross section data of Table 2.

throughout. The cosφ asymmetry must result from a vector polarization in the scattering. Such a vector polarization must depend on spin-orbit effects. Since the multiple scattering calculation ignores these effects, it predicts no cosφ asymmetry.

A nice check on the data is the zero result of the sinφ term (Table 2). The term compares the number scattered up to the number down. Spin-1 double scattering, in the general density matrix formulation, has no sinφ dependence[19], which is what we observed.

The errors in the twelve point and four point phi histograms (after background subtraction) were the square root of the total number of counts under the peak (elastic and background). The errors in the fitted parameters A and B were those necessary to change chi-square by one unit.

We were unable to measure the second scatter cross section to better than 30%, due to poor bunching in the beam from the accelerator. An average beam intensity of 10^4/second corresponds to an instantaneous flux of 2×10^5/second. Poor bunching can increase this flux by factors of 10^2 to 10^3 over small intervals, swamping the secondary beam counters. This 30% uncertainty is within the range of variation predicted by the multiple scattering theory. Unfortunately, without a beam spill monitor more consistent results cannot be obtained.

For the quoted cross section results, chamber efficiencies were calculated using

$$\text{eff} = \frac{\text{analyzed data}}{\text{total triggers}}$$

the beam counts for each run were recorded in a log book during the experiment, and the number of elastic scatters resulted from the background subtractions on the data. The errors given are the square root of the total under the peak with no background subtraction. The normalized cross section, assuming a ten inch effective target is about 1.5 mb/sr overall, agreeing with the equivalent pd experiment at 1 Gev for $-t = .23\ \text{Gev}^2/c^2$ ([7]).

VI. DISCUSSION

We do not find as large a $\cos 2\varphi$ asymmetry (either positive or negative) as that predicted by the multiple scattering theory with no free parameters. The problem could lie within the theory or/and with the background subtractions. In the theory certain parameters are not well known and the calculation neglects the spin-orbit effects, which would be expected to alter the up-right asymmetry as well as account for the observed right-left asymmetry. The background subtractions giving a maximum $\cos 2\varphi$ asymmetry of 67% are consistent within the error bars using various subtraction techniques. If we bolster the positive asymmetry in some way, we also generally make the negative asymmetry less pronounced. The multiple scattering calculation prefers both larger positive and negative asymmetry. The calculation, however, is quite sensitive to the nucleon-nucleon scattering amplitudes (and not so much to the deuteron wave function).

In Figure 19 we show a reasonable fit to our data and to the pd forward cross section data at 1 Gev. Larger real parts of the scattering amplitudes are preferred over those found from nucleon-nucleon scattering. Since the multiple scattering calculation ignores the spin-orbit interaction, it is probably not useful to attempt a "best fit." It is interesting, though, to show the different range of sensitivity involved in fits to the forward cross section compared to fits to the asymmetry data.

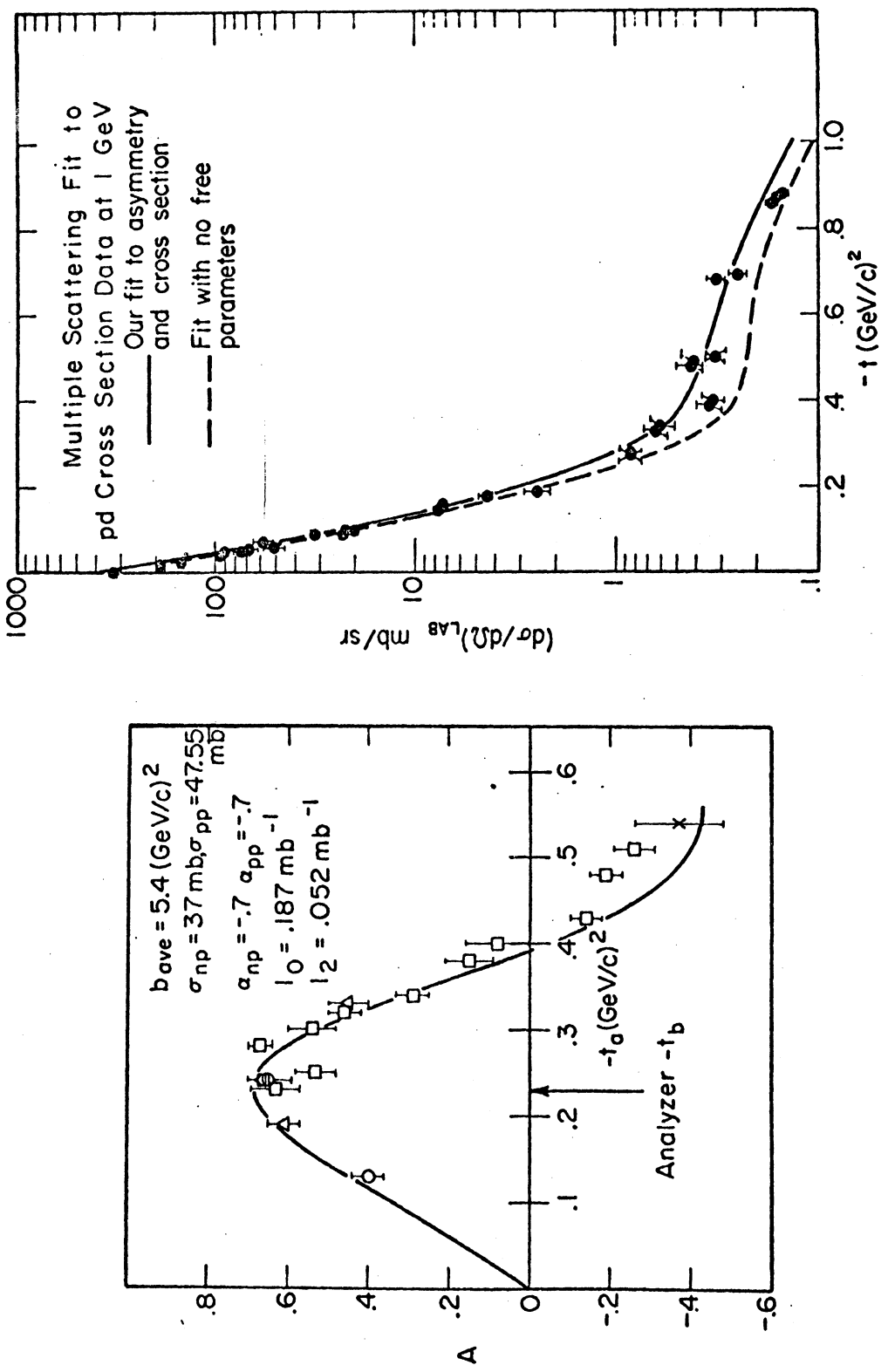

Figure 19. A good fit to the asymmetry and the p-d forward cross section[7].

The cross section data are generally sensitive to a combination of nucleon amplitude slopes and real parts and also to the deuteron D-wave probability. For scattering in the diffraction peak, the slope and the real parts are the determining factor--the other parameter involved, the deuteron monopole form factor S_0, is well known here. In the interference region, larger real parts and larger D-wave probability raise the cross section. Also, Franco[22] has shown that an added proton spin dependence tends to fill in the "dip" region. Thus, one can fit the data fairly well with several combinations of parameters.

For the asymmetry calculation, however, sensitivity to the slopes and to the real parts of the nucleon amplitudes separates. Larger slopes just cause the asymmetry to happen sooner--the slopes shift the cross-over or zero asymmetry point. Larger real parts lower the maximum asymmetry prediction (positive and negative) and do not affect the cross-over. The deuteron parameters S_0 and S_2 also divide rôles. An integral of S_0 results from the double scattering term,

$$I_0 = \int S_0(q') \, e^{-b_{ave} q'^2} \, d^2q' \quad ,$$

and affects the zero asymmetry prediction. The D-wave probability, proportional to S_2^2, influences the size of the asymmetry, but not greatly. A drastic change from 7% to 4% washes out only 10% of the asymmetry maxima.

The D-wave probability of the various proposed deuteron wave functions varies only from 6% to 8%. This lack of sensitivity occurs because scattering in the interference region is mainly D-wave scattering. When more S-wave scattering is introduced there, sensitivity to the D-wave probability increases. The cross section in the interference region is more sensitive to the D-wave probability than is the alignment.

In Figure 20 are fits to the asymmetry and to the 1 Gev pd cross section for different slopes. The Particle Data Group compilation[16] gives the best values for the slopes for protons (neutrons) incident at 1.7 Gev/c as

$$b_{pp} = 6.4 \pm .6 \quad , \quad b_{np} = 4.1 \pm .6 \ (\text{Gev/c})^{-2} \ .$$

That this is in an energy region where the slopes are changing rapidly accounts for the large errors. Both the cross section and the asymmetry calculation reflect an average slope,

$$b_{ave} = (b_{np} + b_{pp})/2 \ .$$

Fits for different real parts of the nucleon amplitudes are shown in Figure 21. The compilation gives

$$\alpha_{pp} = -.2 \pm .2 \quad , \quad \alpha_{np} = -.5 \pm .2 \ .$$

They are rapidly varying in this energy region and can be taken as essentially free parameters. Also, the reported values of α depend on the size of the angular region used to extrapolate the forward cross section to zero angle. This varies considerably. Since the α's

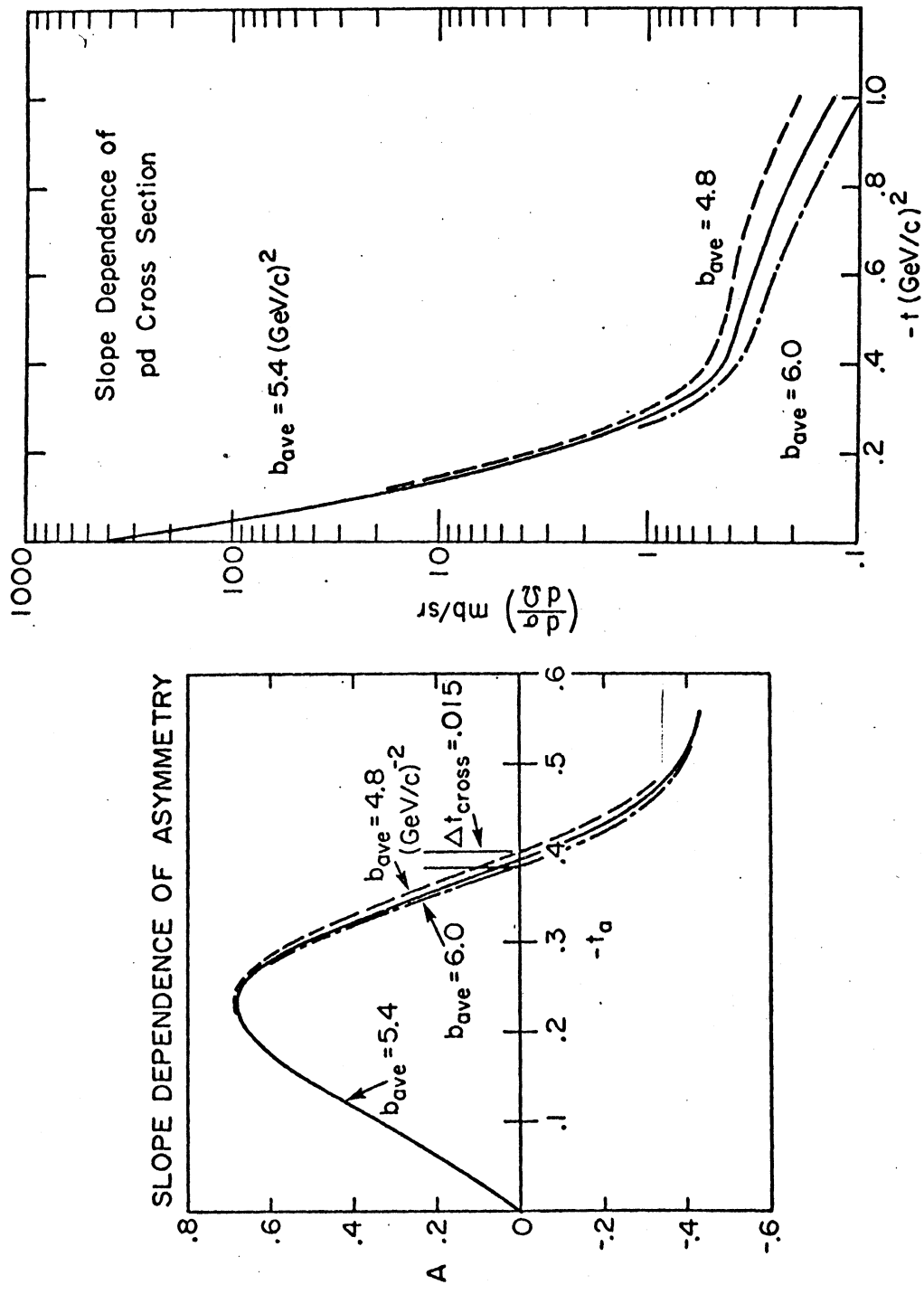

Figure 20. Slope dependence of fits to asymmetry and to the p-d cross section at 1 GeV.

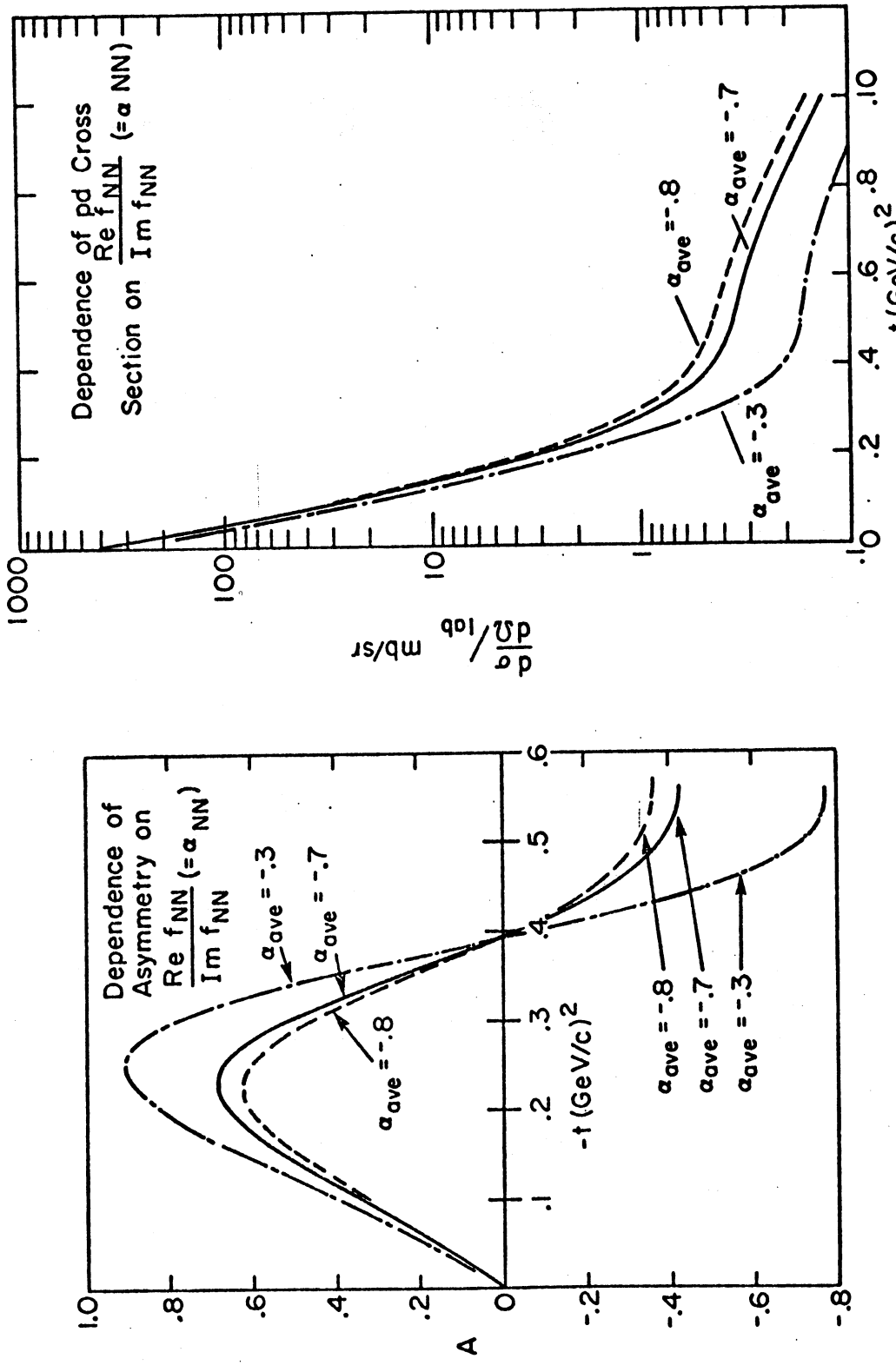

Figure 21. Dependence of multiple scattering model fits on the average real part of the nucleon-nucleon scattering amplitudes.

are not even well known at zero momentum transfer, there is no reason to introduce a t dependence to the real parts, normalizing them to a "known" α at $t\doteq 0$. The asymmetry calculations are sensitive to the average α. Neither calculation cares about the sign. The consensus of np and pp scattering information takes them as negative, so we report them both as negative. If the two α's were of opposite sign, however, they would have little effect on the asymmetry maximum. Thus, if α_{pp} is indeed negative, these calculations suggest that α_{np} is also negative. Since Franco has shown that the introduction of the target proton spin into the theory does things similar to large real parts (filling in the interference region), it is premature to reach any conclusions about the α's.

Our asymmetry data measures the cross-over point as $-t_a = .415 \pm .01$ Gev$^2/c^2$. Using the parameterization for S_0 (Table 1) from the C. N. Bressel, et al. deuteron wave function[23],

$$I_0 = .187 \text{ mb}^{-1}$$

and the predicted cross-over occurs at $t\doteq -.395$, all for the slopes $b_{pp} = 6.4$, $b_{np} = 4.1$. The gaussian[24], Gartenhaus[25], and McGee[27] deuteron wave functions give an integral from 2% to 3% higher, while the Hulthen wave function[26] has an I_0 10% higher than that of Bressel.[28] When this integral is increased, the double scattering term is increased and the asymmetry parameter

$$a_2 \sim \text{Re}\,(M^{\ddagger} + \tfrac{1}{2}Q^{+})\,Q1$$

becomes zero at smaller t. The asymmetry is very sensitive to small changes in the integral, while the cross section is not. For a 3% higher I_0 and the present slopes, the cross-over point becomes $-t_a = .385$. A 10% higher I_0 gives a cross-over point of $-t_a = .375$. Thus, to reach a cross-over point of $-t_a = .41$ with the Hulthen wave function, we would need an average slope of only $b = 3$. For the present slopes, which match the diffraction peak in the cross section nicely (with small α's), the asymmetry cross-over point likes an I_0 10% lower than that of the Bressel deuteron wave function.

Small changes in the D-wave probability affect the cross section more than the asymmetry (Figure 22). As larger α's are used, smaller D-wave probability begins to decrease the asymmetry maximum. Thus, it is possible to use moderately large α's (-.5) and a smaller D-wave probability (5%) to reproduce our data. However, proposed wave functions vary in D-wave probability from 6% to 8%. Also, smaller D-wave raises the I_0 slightly, which is undesirable. In Figure 22, we show the effect of 7.4% D-wave compared to 6%, using the No. 1 and No. 3 potentials of Glendenning-Kramer [14] (with large α's). The asymmetry just isn't that sensitive to the deuteron wave function.

Thus, fits to both the $\cos 2\varphi$ asymmetry and to the forward cross section (using the simple theory without the proton spin) like the slopes found from nucleon-nucleon scattering and prefer larger real parts of the nucleon amplitudes. Larger real parts, though, add to the cross

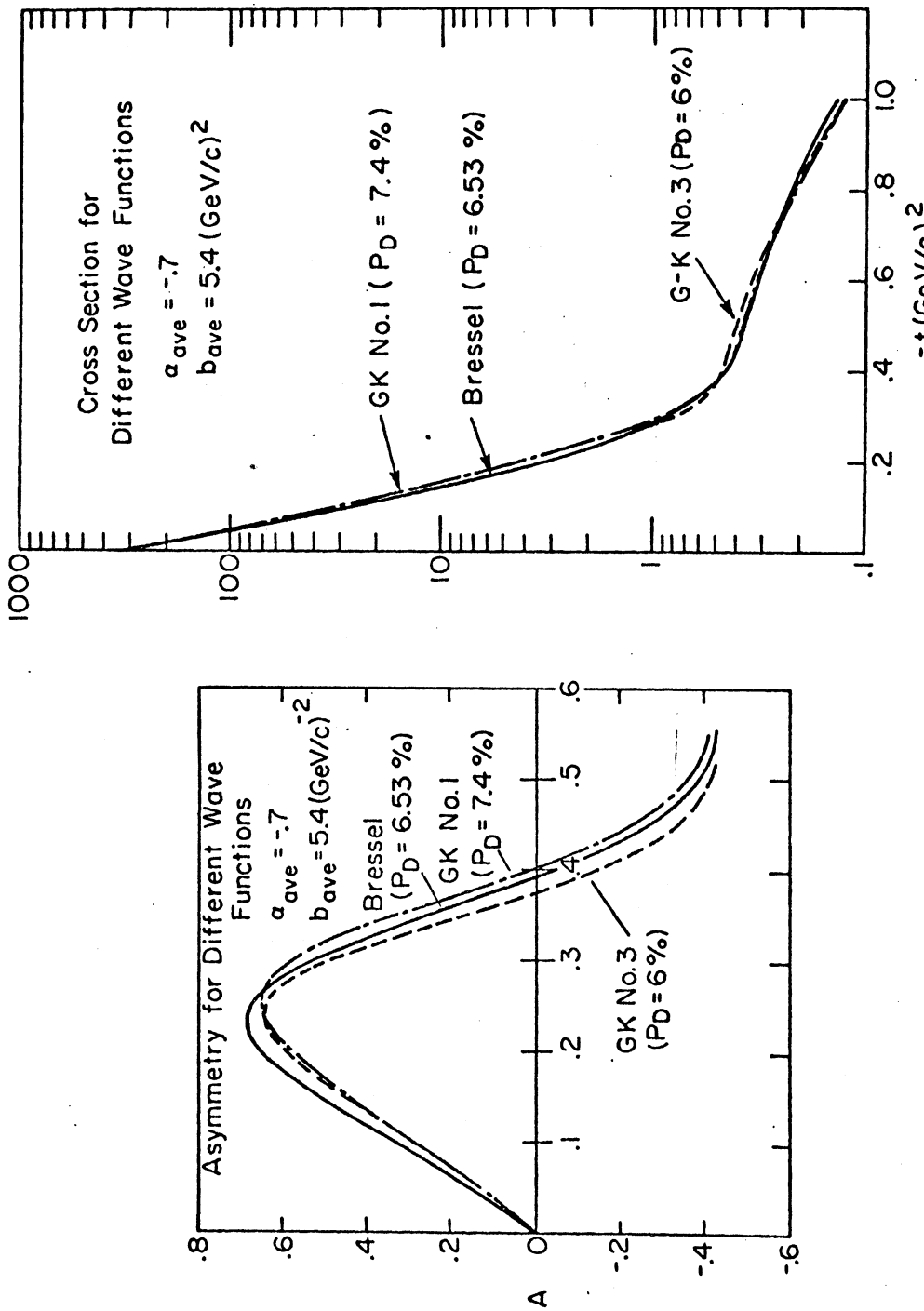

Figure 22. Dependence of the Glauber model fits on the deuteron wave functions of Bressel et al.[23] and of Glendenning-Kramer[14].

section at small t, which is undesirable. Perhaps this is evidence of a slight t-dependence of the α's (smaller α at low t, higher α at large t). Czyz and Lesniak[29] found large real parts ($\alpha = -.33$) preferred with slightly smaller slopes ($b = 5$) in fitting the 1 Gev pHe data with the multiple scattering theory, as did Bassel and Wilkin[30]. Lesniak and Wolek[31] used even smaller slopes ($b = 4.7$) and larger α's ($\alpha = -.4$) to fit the 1 Gev pO and pC data (the pC calculation is high in the double scattering region, presumably due to problems with the carbon wave function). Thus, there is a preference in the Glauber model for larger real parts of the 1 Gev nucleon amplitudes than those reported from nucleon-nucleon scattering. The preferred average slope is about $b = 5$. Also, the asymmetry data likes deuteron wave functions with a smaller double scattering integral (i.e. not the Hulthen wave function). This integral is related to the cross section defect for proton-deuteron scattering[4],

$$I_0 = \frac{8\pi^2}{1-\alpha_{pp}\alpha_{np}} \frac{\sigma_{pn} + \sigma_{pp} - \sigma_{pd}}{\sigma_{pp}\sigma_{pn}} \quad .$$

At 1 Gev[16],

$$\sigma_{pn} = 49.09 \pm .13 \text{ mb} \quad , \quad \sigma_{pp} = 47.55 \pm .06 \text{ mb} \quad ,$$
$$\sigma_{pd} = 83.00 \pm .06 \text{ mb}$$

and

$$I_0 = \frac{.187}{1 - \alpha_{pp}\alpha_{np}} \quad .$$

For large real parts, I_0 would be considerably larger than we find. Unfortunately, the pn cross section is computed

using precisely this integral. An independent determination could be made using a neutron beam, obtaining σ_{np}. Neutron beam measurements have been made at momenta spanning the 1.7 Gev/c value for this experiment [16]:

$$\sigma_{np} = 35.8 \pm 1.6 \text{ mb} \quad \text{at } 1.38 \text{ Gev/c}$$

$$\sigma_{np} = 38.3 \pm 3.2 \text{ mb} \quad \text{at } 2.36 \text{ Gev/c} \quad .$$

If we take $\sigma_{np} = 37$ mb (which we use in our "best fit"), then

$$I_0 = \frac{.07}{1 - \alpha_{pp}\alpha_{np}} \quad ,$$

allowing a value $\alpha_{pp}\alpha_{np} = +.6$ for an I_0 of .18 . Thus, our results imply large α's which bring the σ_{pn} measurements into line with the neutron beam σ_{np} results. The smaller cross section also helps the fit to the pd data.

The simple theory does not predict a $\cos\varphi$ asymmetry. That the asymmetry should be positive at $-t_a = -t_b = .23$ is reasonable, since those deuterons that prefer to scatter right in the first scatter also prefer to scatter to the right in the second scatter for the same scattering angle. One might have expected a more pronounced variation in the polarization in going from a single scattering region to a double scattering region, though. At these energies the pp polarization is 40% and the np polarization is 30% [16]. A 50% deuteron vector polarization (with $P^2 = .25$) does not seem unreasonable. Franco [22] found polarization effects on the order of 20% are expected for the recoil proton in pd S-wave scattering, varying considerably over t. Thus, only the lack of variation in the $\cos\varphi$ term seems unreasonable.

Several points should be made regarding the $\cos\varphi$ asymmetry data. None of the typical vector polarization checks was made, such as rotating the polarization or the apparatus. The right-left asymmetry was not in the raw data, but the background outside the elastic peak consistently showed a negative term. That the background showed the opposite asymmetry suggests that the result is not due to an apparatus malfunction. The $\cos\varphi$ term did not stay constant for different energies at $-t_a = .24$, as did the $\cos 2\varphi$ term.

In summary, our experiment shows that the multiple scattering model does quite well explaining the details of the spin dependence of d-p scattering. As predicted, the D-wave of the deuteron is very important in the break region between single and double scattering. Using the Glauber model, the spin alignment is sensitive both to the free nucleon scattering amplitudes and to the deuteron wave function. Analysis of our results with the Glauber model suggests a preference for large real parts of the scattering amplitudes, although the sizable vector polarization emphasizes the need for more theoretical work. Large alignments are also predicted for higher energies, so this technique can be used there. Finally, strongly vector polarized deuterons, once stripped, provide a source of high energy polarized protons and neutrons. Thus, this technique may be useful in a variety of other experiments.

REFERENCES

1. R. J. Glauber, Lectures in Theoretical Physics, edited by W. E. Brittin et al. (Interscience Publishers, Inc., New York, 1959) Vol. I p. 315; also, R. J. Glauber, Proceedings of the Third International Conference on High Energy Physics and Nuclear Structure, New York, September, 1969, edited by S. Devons (Plenum Press, New York, 1970), p. 207 . The latter contains a history of experiments up to this alignment experiment and a discussion of the theory.
2. H. Palevsky, J. L. Friedes, R. J. Sutter, G. W. Bennett, G. J. Igo, W. D. Simpson, G. C. Phillips, D. M. Corley, N. S. Wall, R. L. Stearns and B. Gottschalk, Phys. Rev. Letters 18, 1200 (1967).
3. E. T. Boschitz, W. K. Roberts, J. S. Vincent, K. Gotow, P. C. Gugelot, C. F. Perdrisat and L. W. Swenson, Phys. Rev. Letters 20, 1116 (1968).
4. H. C. Hsiung, E. Coleman, B. Roe, D. Sinclair and J. Vander Velde, Phys. Rev. Letters 21, 187 (1968).
5. F. Bradamonte, S. Conetti, G. Fidecaro, M. Fidecaro, M. Giorgi, A. Penzo, L. Piemontese, F. Sauli and P. Schiavon, Phys. Letters 28B, 191 (1968).
6. E. Coleman, R. M. Heinz, O. E. Overseth and D. E. Pellet, Phys. Rev. Letters 16, 761 (1966).
7. G. W. Bennett, J. L. Friedes, H. Palevsky, R. J. Sutter, G. J. Igo, W. D. Simpson, G. C. Phillips, R. L. Stearns and D. M. Corley, Phys. Rev. Letters 19, 387 (1967).

8. E. Coleman and T. G. Rhoades (private communication).

9. D. R. Harrington, Phys. Rev. Letters 21, 1496 (1968).

10. V. Franco and R. J. Glauber, Phys. Rev. Letters 22, 370 (1969).

11. H. C. Hsiung, University of Michigan Report COO-1112-7 (1969).

12. D. R. Harrington, Phys. Letters 29B, 188 (1969).

13. G. Chew, Phys. Rev. 74, 809 (1948).

14. N. K. Glendenning and G. Kramer, Phys. Rev. 126, 2159 (1962).

15. J. C. Vander Velde, Phys. Rev. 173, 1544 (1968), footnote 10.

16. O. Benary, L. R. Price and G. Alexander, Particle Data Group, NN and ND Interactions (above .5 GeV/c)--A Compilation, UCRL - 20000 NN, August 1970.

17. G. Alberi, L. Bertocchi and G. Bialkowski, "High Energy Deuteron-Deuteron Elastic Scattering and Quadrupole Deformation," ICTP preprint (1969).

18. See, for example, W. S. C. Williams, An Introduction to Elementary Particles, New York, Academic Press (1961), page 172.

19. W. Lakin, Phys. Rev. 98, 139 (1955); H. P. Stapp, UCRL - 3098, August 1955 (unpublished); S. E. Darden, Am. J. Phys. 35, 727 (1967).

20. L. Wolfenstein (private communication); also, the particular parameterization of the cross section on page 19 is due to Wolfenstein.

21. R. E. Mischke, T. J. Devlin, W. Johnson, J. Norem, K. Vosburgh and W. Schimmerling, Phys. Rev. Letters 25, 1724 (1970).

22. V. Franco, Phys. Rev. 21, 1360 (1968).

23. C. N. Bressel, A. K. Kerman and B. Rouben, Nuclear Phys. A124, 624 (1969).

24. M. Verde, Helv. Phys. Acta 22, 339 (1949).

25. M. Moravcsik, Nuclear Phys. 7, 113 (1958), approximation II.

26. Ibidem, approximation I.

27. I. J. McGee, Phys. Rev. 151, 772 (1966).

28. The integrals of these wave functions were presented in F. Bradamante, G. Fidecaro, M. Fidecaro, M. Giorgi, P. Palazzi, A. Penzo, L. Piemontese, F. Sauli, P. Schiavon and A. Vascotto, Phys. Letters 32B, 303 (1970).

29. W. Czyz and L. Lesniak, Phys. Letters 24B, 227 (1967).

30. R. Bassel and C. Wilkin, Phys. Rev. Letters 18, 871 (1967).

31. L. Lesniak and H. Wolek, Nuclear Phys. A125, 665 (1969).